HHS Public Access

Author manuscript

Mol Cell. Author manuscript; available in PMC 2021 January 16.

Published in final edited form as:

Mol Cell. 2020 January 16; 77(2): 384–394.e4. doi:10.1016/j.molcel.2019.10.031.

HMCES functions in the alternative end-joining pathway of the DNA DSB repair during class switch recombination in B cells.

Vipul Shukla[1], **Levon Halabelian**[2], **Sanjana Balagere**[1], **Daniela Samaniego-Castruita**[1], **Douglas E. Feldman**[3], **Cheryl H Arrowsmith**[*,2,4,5], **Anjana Rao**[*,ǂ,1,6,7], **L. Aravind**[*,8]

[1]Division of Signaling and Gene Expression, La Jolla Institute for Immunology, 9420 Athena Circle, La Jolla, California, 92037, USA.

[2]Structural Genomics Consortium, University of Toronto, Toronto, ON, M5G 1L7, Canada.

[3]Department of pathology, University of Southern California, Keck School of Medicine, Los Angeles, CA 93033

[4]Department of Medical Biophysics, University of Toronto, Toronto, ON, M5G 1L7, Canada.

[5]Princess Margaret Cancer Centre, University Health Network, Toronto, ON, M5G 2M9, Canada.

[6]Department of Pharmacology and Moores Cancer Center, University of San Diego, California; 9500 Gilman Drive, La Jolla, California, 92093, USA.

[7]Sanford Consortium for Regenerative Medicine; 2880 Torrey Pines Scenic Drive, La Jolla, California, 92037, USA.

[8]National Center for Biotechnology Information, National Library of Medicine, National Institutes of Health, Bethesda, MD 20894, USA.

Summary

HMCES (5hmC binding, ES-cell-specific-protein), originally identified as a protein capable of binding 5-hydroxymethylcytosine (5hmC), an epigenetic modification generated by TET proteins, was previously reported to covalently crosslink to DNA at abasic sites via a conserved cysteine. We show here that *Hmces*-deficient mice display normal hematopoiesis without global alterations in 5hmC. HMCES specifically enables DNA double-strand break repair through the microhomology-mediated Alternative-End-Joining (Alt-EJ) pathway during class switch recombination (CSR) in B cells, and HMCES deficiency leads to a significant defect in CSR.

[*]Corresponding authors: Dr. L. Aravind (aravind@ncbi.nlm.nih.gov), Dr. Anjana Rao (arao@lji.org), Dr. Cheryl H. Arrowsmith (Cheryl.Arrowsmith@uhnresearch.ca). [ǂ]Lead contact: Dr. Anjana Rao (arao@lji.org).

Author Contributions

V.S. conceptualized the experiments, acquired and analyzed the data, and wrote the manuscript. L.H. performed structural studies of the HMCES protein, drafted parts of the manuscript, helped with the interpretation of data and reviewed the manuscript. S.B. performed cloning of the HMCES variants. D.S.C. performed switching experiments in primary B cells. D.E.F. provided the *Hmces*-deficient mice used in the study. L.A. contributed to conceptualization of the experiments, discussion of the data and review of the manuscript. C.H.A. supervised the structural studies of HMCES, interpretation of the data and reviewing the manuscript. A.R. supervised the studies, conceptualized the experiments, helped with the interpretation of data and wrote the manuscript.

Declaration of Interests. The authors declare no competing interests.

HMCES mediates Alt-EJ through its SOS-response-associated-peptidase domain (SRAPd), a function that requires DNA binding but is independent of its autopeptidase and DNA-crosslinking activities. We show that HMCES is recruited to switch regions of the immunoglobulin locus and provide a potential structural basis for the interaction of HMCES with long DNA-overhangs generated by Alt-EJ during CSR. Our studies provide further evidence for a specialized role for HMCES in DNA repair.

Graphical Abstract

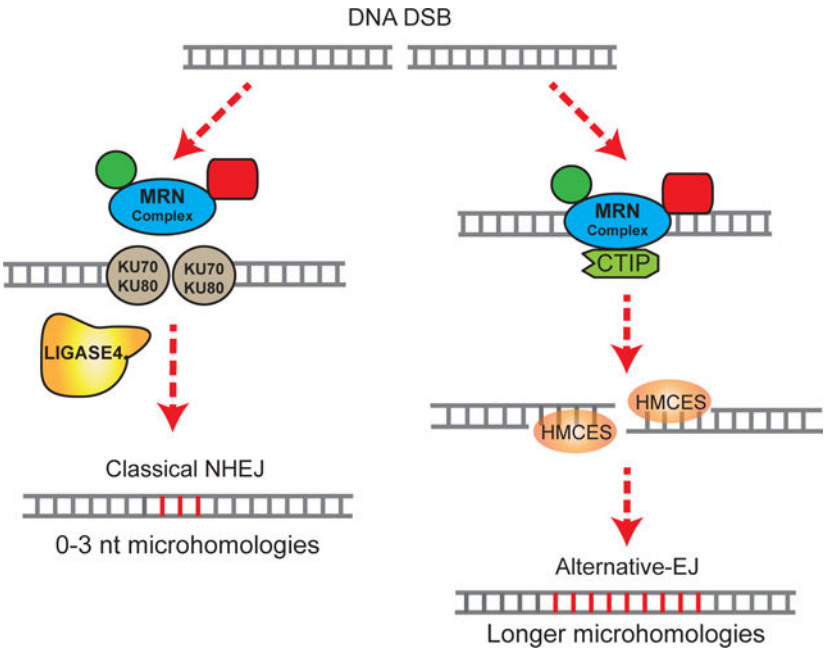

eTOC blurb:

HMCES (5hmC binding, ES-cell-specific-protein), originally identified to bind 5-hydroxymethylcytosine (5hmC), was recently reported to covalently crosslink to DNA at abasic sites. Shukla et al. show that HMCES specifically enables DNA double-strand break repair through the microhomology-mediated Alternative-End-Joining (Alt-EJ) pathway during class switch recombination (CSR) in B cells.

Keywords

HMCES; TET proteins; oxidized methylcytosine; CSR; DNA DSB repair; Alternative end-joining

Introduction

5-Hydroxymethylcytosine binding, ES cell specific protein (HMCES) is the sole mammalian representative of a superfamily of proteins that includes *E.coli* YedK(Aravind et al., 2013). It is highly conserved among bacteria with sporadic appearances in certain phages(Aravind et al., 2013). This superfamily has operonic associations with the bacterial SOS DNA damage response, mutagenic translesion DNA polymerases, non-homologous DNA-ending-joining

networks which employ Ku and an ATP-dependent ligase, and other repair systems (Aravind et al., 2013). The superfamily is characterized by the presence of an SOS response-associated peptidase (SRAP) domain with a novel thiol autopeptidase activity, whose active site in human HMCES is comprised of the catalytic triad residues C2, E127 and H210(Aravind et al., 2013; Halabelian et al., 2019; Kweon et al., 2017; Mohni et al., 2019; Thompson et al., 2019). HMCES, the only well-conserved mammalian protein with a SRAP domain, also functions as an autopeptidase(Kweon et al., 2017), and bears an additional C-terminal extension, which has been implicated in autoinhibition and binding other DNA-repair proteins (e.g. PCNA)(Kweon et al., 2017; Mohni et al., 2019).

Consistent with a conserved role in the response to DNA damage, human HMCES was recently shown to bind and covalently crosslink via its SRAP domain to abasic sites at stalled replication forks(Halabelian et al., 2019; Mohni et al., 2019; Thompson et al., 2019). Both binding and crosslinking involved the autopeptidase catalytic triad residues C2, E127 and H210(Mohni et al., 2019), with the crosslink itself taking the form of a thiazole ring constituted from cysteine C2 of the catalytic triad (after autoproteolytic cleavage of the N-terminal methionine) and the deoxyribose of the abasic site(Halabelian et al., 2019; Mohni et al., 2019; Thompson et al., 2019). HMCES-deficient cells display an increase in DNA double strand breaks (DSBs) and hypersensitivity to ionizing radiation, short wavelength UV and the alkylating agent methyl methanesulfonate(Mohni et al., 2019). Since HMCES was not required for DNA DSB repair through homologous recombination or the canonical/classical Non-homologous End-Joining pathway (c-NHEJ), the increase in DNA DSBs in HMCES-deficient cells was suggested to occur as a consequence of error-prone processing of abasic sites in DNA(Mohni et al., 2019).

Hmces mRNA expression is strongly induced in activated B cells, which undergo rapid proliferation and acquire mutations at their Immunoglobulin (Ig) loci through the cytosine deamination activity of the enzyme AID (Activation-Induced cytidine deaminase)(Alt et al., 2013; Chang et al., 2017; Stavnezer and Schrader, 2014; Xu et al., 2005). AID-driven mutations in Ig loci result in somatic hypermutation (SHM), single nucleotide changes in Ig variable regions that alter Ig affinity, and also promote the generation of DNA double-strand breaks (DNA DSBs) to induce class switch recombination (CSR)(Alt et al., 2013; Chang et al., 2017; Stavnezer and Schrader, 2014; Xu et al., 2005). During CSR, DNA DSBs generated at switch regions located 5’ of the coding regions of distinct Ig isotypes are annealed by one of two redundant DNA DSB repair pathways, the well characterized c-NHEJ pathway and the less well described but robust alternative end joining pathway (Alt-EJ)(Alt et al., 2013; Boboila et al., 2010; Chang et al., 2017; Stavnezer and Schrader, 2014; Yan et al., 2007). DNA DSB repair by c-NHEJ involves limited processing of DNA ends and few or no sequence microhomologies, while the Alt-EJ pathway is mediated through more elaborate strand resection, generation of ssDNA overhangs and frequent use of microhomologies at the joined ends(Alt et al., 2013; Chang et al., 2017; Lee-Theilen et al., 2011; Stavnezer and Schrader, 2014).

HMCES was originally identified by mass spectrometry as a protein that preferentially bound to oligonucleotides containing the oxidised methylcytosine bases 5-hydroxymethylcytosine (5hmC), 5-formylcytosine (5fC) and 5-carboxylcytosine (5caC),

over binding to identical oligonucleotides containing unmodified cytosine or 5-methylcytosine (5mC) in the CpG sequence context(Spruijt et al., 2013). Oxidised methylcytosines are produced by enzymes of the TET family, Fe(II) and α-ketoglutarate-dependent dioxygenases that sequentially oxidize the methyl group of 5mC to 5hmC, 5fC and 5caC(Cimmino et al., 2011; Ito et al., 2011; Iyer et al., 2009; Pastor et al., 2013; Tahiliani et al., 2009). However, we show here that despite the importance of TET proteins in normal hematopoiesis, *Hmces*-deficient mice(Kweon et al., 2017) showed no obvious defects in hematopoiesis and no alterations in global 5hmC levels in bone marrow cells. Rather, the major defect that we observed was a decrease in class switch recombination in mature activated B cells. We demonstrate a novel function for HMCES in regulating DNA DSB repair through the microhomology-mediated Alt-EJ pathway during CSR, and provide evidence that the role of HMCES in Alt-EJ is independent of its ability to form DNA-protein crosslinks (DPCs)(Mohni et al., 2019). Together, our studies define additional roles of this highly conserved protein in eukaryotic DNA damage and repair responses in activated B cells.

Results

Hmces-deficient mice show normal hematopoiesis

Hmces mRNA is expressed across different hematopoietic lineages (Immgen database; Figure S1A). To assess the potential biological role of HMCES in hematopoietic development and function, we analyzed hematopoiesis in 6–8 week old HMCES-deficient mice. Compared with $Hmces^{+/+}$ littermate control mice, $Hmces^{-/-}$ mice showed no significant alterations in the frequencies of LSK (Lineage $(Lin)^-$ $Sca1^+$ $cKit^+$) and LK (Lin^- $cKit^+$) progenitor cell subsets, or the frequencies of differentiated B, T and myeloid cells in the bone marrow (BM) and spleen (Figures S1B–S1D).

Notably, we observed a slight but significant increase in the absolute numbers of LSK, LK and early B cell progenitors (pre-B cells) in bone marrow of $Hmces^{-/-}$ mice compared with $Hmces^{+/+}$ controls (Figures S1E, S1F). However, there was no corresponding increase in the frequency or numbers of B cells, CD4 and CD8 T cells or myeloid cells in the spleen (Figure S1G, S1H), and serial replating assays showed no significant differences in colony-forming ability of sorted LSK cells from $Hmces^{+/+}$ and $Hmces^{-/-}$ mice (Figure S2A). Moreover, competitive mixed BM chimeras generated by injecting 1:1 mixtures of $CD45.2^+$ $Hmces^{+/+}$ or $Hmces^{-/-}$ BM cells with CD45.1.2 WT BM cells into lethally irradiated $CD45.1^+$ recipient mice revealed no significant differences in the relative contributions of $Hmces^{+/+}$ versus $Hmces^{-/-}$ cells to different hematopoietic lineages in the transplanted mice (Figures S2B, S2C). Although *Hmces*-deficient ES cells have been reported to show decreased 5hmC levels(Kweon et al., 2017), we did not observe any obvious differences in the global levels of 5hmC by dot blot analysis of bisulfite-treated DNA from bone marrow cells of $Hmces^{+/+}$ and $Hmces^{-/-}$ mice, using a highly specific antibody to cytosine-5-methylene sulfonate (CMS)(Huang et al., 2012; Ko et al., 2010) (Fig S2D). Together, these results demonstrate that loss of HMCES in hematopoietic-lineage cells does not lead to major alterations in global 5hmC levels in the bone marrow or in hematopoietic differentiation or function.

HMCES deficiency is associated with a significant defect in CSR in primary B cells

Hmces mRNA expression is high in germinal center (GC) B cells and moderately high in plasma cells compared to pro-B cells, follicular (FO) and marginal zone (MZ) B cells (Immgen database, Figure S1A). Moreover, *Hmces* mRNA was strongly induced in a subset of GC B lymphocytes (CC, centrocytes; CB, centroblasts) undergoing proliferation, activation and differentiation (Immgen database, Figure 1A). Indeed, GC B cells isolated from mice immunized with sheep red blood cells (SRBCs) showed a ~9-fold increase in expression of *Hmces* mRNA by quantitative-real time PCR compared with non-GC, naïve B cells from the same mice (Figure 1B).

However, loss of *Hmces* did not alter the generation of GC B cells in response to footpad immunization with 4-hydroxyl nitrophenyl (NP)-conjugated ovalbumin (NP-OVA) (Figures S2E, S2F). Moreover, the frequencies of NP hapten-specific GC B cells, $CD138^{+}$ differentiating cells and the ratio of centrocytes ($CXCR4^{lo}CD86^{hi}$-light zone) to centroblasts ($CXCR4^{lo}CD86^{hi}$-dark zone) also appeared comparable between Hmces-deficient (*Hmces* $^{-/-}$), wild-type (WT) (*Hmces*$^{+/+}$) and heterozygous (*Hmces*$^{+/-}$) littermate mice (Figures S2G, S2H, S2I). The only consistent and statistically significant difference observed post-immunization was a decrease in immunoglobulin (Ig) isotype class switching from IgM to IgG1 in *Hmces*$^{-/-}$ GC B cells compared with *Hmces*$^{+/+}$ or *Hmces*$^{+/-}$ GC B cells (Figures 1C, 1D).

To confirm the defect in CSR, we stimulated primary B cells isolated from *Hmces*$^{+/+}$ and *Hmces*$^{-/-}$ mice with anti-CD40, Interleukin-4 (IL-4), Interleukin-5 (IL-5) and Transforming Growth Factor β (TGFβ), and assessed their Ig class switching from IgM to IgG1 or IgA at various time points. Consistent with the observation of decreased CSR *in vivo*, *in vitro* stimulated *Hmces*-deficient cells showed a slight but significant reduction in CSR to both IgG1 and IgA isotypes at later times of stimulation (Figures 2A, 2B, 2C). Similar defects in CSR were observed upon stimulation of *Hmces*$^{-/-}$ B cells with anti-CD40 and Interleukin-4 (IL-4), which induces switching to IgG1 and IgE isotypes (Figures 2D, 2E). However, isotype switching to IgG3 and IgG2b were not affected in *Hmces*$^{-/-}$ B cells stimulated with Lipopolysaccharide (LPS) (Figures 2F, S3A). Importantly, the defect in CSR in *Hmces*$^{-/-}$ B cells was not due to altered expression of the *Aicda* gene that encodes the AID cytidine deaminase, or to changes in germline transcription of Igμ and Igγ1 regions, 48 hours post-stimulation with anti-CD40 and IL-4 (Figures S3B). Also, *Hmces*$^{-/-}$ B cells proliferated at comparable levels with *Hmces*$^{+/+}$ B cells stimulated under several conditions at various different time points, as measured by dilution of Cell Trace Violet dye (Figures S3C, S3D, S3E).

HMCES contributes to CSR in the CH12 B cell line

To understand the mechanisms by which HMCES regulates CSR in B cells, we used CH12F3 (CH12) cell line which represents a useful experimental model system more amenable to genetic and biochemical manipulations than primary B cells. CH12 cells undergo Ig isotype switching from IgM to IgA upon stimulation with anti-CD40, IL-4 and TGF-β, and constitute a valuable model system that has been used extensively to gain mechanistic insights into CSR(Lee-Theilen et al., 2011; Nakamura et al., 1996).

To analyze the mechanistic role of HMCES in CSR, we generated *Hmces*-deficient clones of the CH12 mouse B cell line using CRISPR-Cas9 mediated targeting. We targeted exon 2, the first coding exon of *Hmces*, with two guide RNAs (Figure S4A, *left*), and confirmed disruption of the open reading frame and loss of HMCES protein in two clones derived from single cells, ΔHMCES H3 and H23 (Figures S4A, S4B). As also observed with a slightly longer latency in primary GC B cells from *Hmces*$^{-/-}$ mice(Figure 2), ΔHMCES CH12 clones showed a significant reduction in CSR at 48 hours (~20%; Figure S4C) and a much more pronounced defect at 72 hours after stimulation (~50%; Figures 3A, 3B). The reduction in CSR was not due to decreased expression of μ and α germline transcripts or decreased *Aicda* expression, which were comparable between WT and ΔHMCES CH12 cells (Figure S4D). As judged by flow cytometry, full-length (FL) human HMCES was expressed at moderately higher levels than endogenous HMCES after transduction of either WT or ΔHMCES CH12 cells with a lentivirus encoding HMCES followed by GFP from an internal ribosome entry site (IRES) cassette (Figure S4E, *top diagram and bottom right panel*). Reconstitution of ΔHMCES CH12 cells with FL HMCES restored CSR to levels higher than WT CH12 expressing empty vector and similar to WT CH12 cells ectopically expressing FL HMCES protein, 72 hours after stimulation (Figures 3C, 3D). Notably, ectopic expression of FL HMCES in WT CH12 cells also significantly accelerated the kinetics (Figure S4F) of CSR.

Recent studies have identified important features of HMCES protein including the N-terminal SRAP domain (SRAPd, HMCES 1–270), the catalytic triad residues C2, E127 and H210 required for autopeptidase activity(Aravind et al., 2013; Halabelian et al., 2019; Kweon et al., 2017), the R98 and R212 residues required for binding to many different forms of completely and partially single stranded (ss) DNA (Mohni et al., 2019) and the C-terminal region containing three PIP (PCNA-interacting protein) motifs that can bind PCNA and other DNA repair regulators(Boehm and Washington, 2016) and recruit HMCES to replication forks(Mohni et al., 2019) (Figure 3E). Cysteine residue 2 is also the site through which HMCES crosslinks to the abasic site of DNA(Halabelian et al., 2019; Mohni et al., 2019; Thompson et al., 2019).

To determine which of these features were required for HMCES-mediated potentiation of CSR, we used the lentiviral expression plasmid described above (Figure S4E, *upper panel*) to transduce ΔHMCES clones H3 and H23 with C-terminally truncated HMCES (1–270 aa) representing the SRAP domain alone(Aravind et al., 2013; Halabelian et al., 2019; Kweon et al., 2017; Mohni et al., 2019), the HMCES C2A mutant that lacks autopeptidase activity(Kweon et al., 2017) and the activity to crosslink at abasic DNA sites(Mohni et al., 2019) and the HMCES R212A mutant that completely abolishes the ability of HMCES to bind DNA containing stretches of single strandedness (Mohni et al., 2019). The transduced cells were stimulated with anti-CD40, IL-4, and TGFβ, and the extent of IgM to IgA switching in WT and ΔHMCES cells expressing the HMCES variants was compared by flow cytometry in cells gated on GFP expression. As expected, cells expressing the HMCES C2A mutant showed the highest median fluorescence intensity for HA compared to other HMCES variants (Figure S5A); this mutant lacks autopeptidase activity directed at the N-terminal methionine and so cannot liberate the N-terminal HA tag. Using an antibody which recognizes an internal epitope located between amino acids 111 and 153 of human HMCES,

we confirmed that the different HMCES variants were expressed at similar levels in WT and ΔHMCES CH12 cells (Figure S5B). Notably, both the HMCES SRAPd (HMCES 1–270) and C2A mutants restored CSR in ΔHMCES CH12 cells (Figures 3F, 3G), indicating that the C-terminal region, autopeptidase activity and abasic site DNA-crosslinking activity were likely not required for the ability of HMCES to potentiate CSR. In contrast, the R212A mutant that lacks the ability to bind to DNA was not able to rescue the defect in CSR in HMCES-deficient CH12 cells (Figures 3F, 3G), suggesting that the DNA binding activity of HMCES is required for its role in CSR.

HMCES functions in the Alt-EJ pathway

HMCES is the mammalian ortholog of the prokaryotic YedK protein that functions in the bacterial SOS DNA damage response(Aravind et al., 2013), and human HMCES is involved in the resolution of stalled replication forks(Mohni et al., 2019). Since our studies showed no obvious changes in proliferation, germline transcription or *Aicda* expression in HMCES-deficient B cells but we nevertheless observed a requirement for HMCES DNA binding in CSR, we investigated a direct involvement of HMCES in DNA repair during CSR. CSR occurs when DNA double strand breaks (DSB) in switch regions located 5' of constant coding regions of Ig isotypes are stitched together by the DNA DSB repair machinery(Alt et al., 2013; Chang et al., 2017; Stavnezer and Schrader, 2014). The newly formed junctions between two switch regions are generated either by the action of the c-NHEJ pathway, which yields end joins with little to no sequence microhomologies, or the Alt-EJ pathway that uses DNA strand resection and substantial microhomologies to join DSBs(Alt et al., 2013; Chang et al., 2017; Stavnezer and Schrader, 2014).

We amplified and sequenced the Switch μ and Switch α (Sμ–Sα) junctions resulting from CSR in HMCES-sufficient and -deficient CH12 cells. There was a very strong change in the pattern of microhomologies at Sμ - Sα junctions in HMCES-deficient compared to WT CH12 cells (Figures 4A, 4B, S6A). In WT CH12 cells, 45% and 55% of Sμ–Sα junctions showed microhomologies of 0–3 and >3 nucleotides, respectively (Figure 4B, *left*; Supplementary Table 1a). In contrast, the vast majority (97%) of Sμ–Sα junctions sequenced from HMCES-deficient CH12 cells showed microhomologies of <3 nucleotides (Figure 4B, *middle*). Importantly, reconstitution of HMCES-deficient cells with FL HMCES protein skewed the pattern even more strongly towards longer microhomologies with only 5 out of 17 sequences (~29%) displaying microhomologies of ≤3 nucleotides (Figures 4A, 4B, *right*). Similarly, analysis of Switch μ and Switch γ1 (Sμ–Sγ1) junctions in *Hmces*$^{-/-}$ primary B cells stimulated with anti-CD40 and IL-4 for 96 hours revealed a striking loss of microhomology usage compared with *Hmces*$^{+/+}$ B cells (Figures 4C, 4D, Supplementary Table 1b). Together, these results suggest that HMCES functions primarily in the Alt-EJ pathway, which generates longer microhomologies (>3 nucleotides) than the classical c-NHEJ pathway.

To confirm these findings in an independent system, we deleted HMCES protein using CRISPR-Cas9 in human U2OS cells harboring GFP reporters for c-NHEJ (the EJ5-GFP cell line) and Alt-EJ (the EJ2-GFP cell line)(Gunn and Stark, 2012), referred to here as U2OS c-NHEJ and U2OS Alt-EJ respectively. We confirmed the loss of HMCES in these isogenic

clones by western blotting (Figure S6B). Consistent with the switch junction analysis, loss of HMCES led to an ~50% decrease in the frequency of GFP-positive cells in ΔHMCES compared with WT U2OS Alt-EJ reporter cells (Figures 4E, S6C), with no significant difference in the frequency of GFP-positive cells in ΔHMCES compared with WT U2OS c-NHEJ reporter cells (Figure 4E). The magnitude of the decrease in DNA repair in ΔHMCES U2OS Alt-EJ reporter cells is similar to that previously reported in U2OS Alt-EJ reporter cell lines with profound depletion of CTIP, an important factor in Alt-EJ(Howard et al., 2015; Lee-Theilen et al., 2011). We also tested the sensitivity of WT and ΔHMCES CH12 cells to X-irradiation, which induces DNA DSBs. At 2 hours post irradiation with 500 rads of X-rays, ΔHMCES CH12 cells showed increased staining for the DNA DSB marker, γH2AX, compared with WT CH12 cells (Figure S6D); a similar increase in sensitivity to ionizing radiation was previously reported for HMCES-deficient U2OS cells(Mohni et al., 2019). Collectively, these results highlight a novel function for HMCES in the Alt-EJ pathway of CSR.

Genetic disruption of the c-NHEJ pathway leads to a marked loss of DNA DSB repair in HMCES-deficient cells

c-NHEJ and Alt-EJ pathways function redundantly in CSR, with KU and LIGASE4 functioning specifically in c-NHEJ(Alt et al., 2013; Boboila et al., 2010; Chang et al., 2017). We asked whether disruption of the c-NHEJ pathway in HMCES-deficient cells would lead to more pronounced defects in CSR than observed with HMCES deficiency alone. We achieved robust depletion of KU70 in CH12 cells with lentiviral vectors encoding shRNA against KU70 (shKU70) (Figure S6E). As reported previously, depletion of KU70 resulted in an ~60% decrease in CSR in wildtype CH12 cells(Lee-Theilen et al., 2011), compared with cells transduced with non-targeting control shRNA (shNT) (Figures 5A, 5B, *left bars and panels*). Notably, depletion of KU70 in HMCES-deficient cells led to an overall ~90% reduction in CSR, a result significantly more striking than the 50–60% decrease observed in cells deficient in HMCES or KU70 alone (Figures 5A, 5B).

Since we were unable to obtain effective shRNA-mediated knockdown of LIGASE4, we deleted LIGASE4 using CRISPR-Cas9 mediated targeting in HMCES-sufficient or -deficient CH12 clones (Figure S6F). As reported previously (Han and Yu, 2008), LIGASE4 deletion led to an ~50% decrease in CSR in wildtype CH12 cells, whereas double deletion of HMCES and LIGASE4 led to a dramatic (~80% to 90%) reduction (Figures 5C, 5D). This decrease was highly significant compared with that observed in HMCES or LIGASE4 deficient cells alone (Figures 5C, 5D).

Given our findings that HMCES mainly participates in the Alt-EJ pathway of DNA DSB repair, we reasoned that depletion of another Alt-EJ component may not have any additional effect on CSR in HMCES-deficient CH12 cells. To test this, we depleted CTIP using shRNAs (shCTIP-1 and shCTIP-2) in WT and HMCES-deficient CH12 cells. We observed robust knockdown of CTIP protein expression using the shRNAs (Figure S6G) that was accompanied by an ~40–50% decrease in CSR in WT CH12 cells (Figures 5E, 5F), as reported previously(Lee-Theilen et al., 2011). Consistent with our hypothesis, depletion of

CTIP in HMCES-deficient CH12 cells did not lead to a further decrease in CSR (Figures 5E, 5F), as would be expected if HMCES and CTIP functioned in the same pathway.

Together, these data demonstrate that HMCES functions uniquely through the Alt-EJ pathway in CSR. HMCES-mediated, microhomology-directed Alt-EJ and c-NHEJ are redundant but distinct pathways involved in DNA DSB repair during CSR. Thus, the compounded loss of HMCES and the KU70 or LIGASE4 proteins essential for c-NHEJ causes a dramatic reduction in CSR, whereas the dual loss of HMCES and the Alt-EJ factor CTIP does not.

HMCES binds switch regions and protects ssDNA overhangs during CSR

We tested the ability of HMCES to bind switch regions in CH12 cells undergoing CSR in CH12 cells transduced with a non-targeting shRNA (shNT) and stimulated with anti-CD40, IL-4 and TGFβ (CIT) for 48 hours. Chromatin immunoprecipitation for endogenous HMCES protein showed moderate (~2-fold) enrichment of HMCES at the switch μ (Sμ) region over the background observed in HMCES-deficient, CIT-stimulated CH12 cells (Figure 6A, *compare red and blue bars*). This enrichment increased significantly, to ~9-fold over background, in CH12 cells transduced with shRNA against KU70 to minimize c-NHEJ (Figure 6A, *compare green with red and blue bars*). No increase in HMCES occupancy was observed at Sμ regions in unstimulated CH12 cells or at an adjacent intronic μ enhancer region with or without stimulation (Figure 6A).

How might HMCES promote Alt-EJ over c-NHEJ? In our recent crystal structures of SRAPd bound to dsDNA containing a small (3 nucleotide) 3’ overhang(Halabelian et al., 2019), we showed that HMCES can recognize 3’ and 5’ overhang DNA structures in a sequence independent manner(Halabelian et al., 2019). To explore alternative HMCES-DNA interactions and to test the ability of HMCES to accommodate longer 3’ overhangs involved in Alt-EJ, we co-crystallized SRAPd with a palindromic DNA molecule containing a core double-stranded region flanked by five-nucleotide overhangs on each 3’ end (SRAPd_P5nt; Figure 6B). During crystallization of this mixture (which occurred over 25 days) the 3’ overhangs of the DNA were truncated to three and four nucleotides on each end of the DNA molecule, likely due to the presence of a minor exonuclease contaminant in the protein preparation. The resulting crystal lattice shows each 3’ end of DNA bound to a separate SRAPd. Compared to the previously published HMCES-DNA structures, SRAPd_P5nt shows how HMCES interacts with a 4-nucleotide overhang. The 3’ ends of both the 3-nucleotide and the 4-nucleotide overhangs are bound in the catalytic triad pocket, anchored by a hydrogen bond to conserved residue H210, as seen for the previous SRAPd-DNA structures(Halabelian et al., 2019) (Figure 6B). Several differences were observed between 3-nucleotide versus 4-nucleotide overhang interaction modes with the HMCES SRAPd in SRAPd_P5nt: in the case of the 4-nucleotide overhang, the Phe92 side chain stacks onto the pentose sugar of thymine nucleotide at position 9 (T9), whereas in the 3-nucleotide overhang conformation, the Phe92 side chain stacks edge-to-face with the thymine base (T9). Furthermore, the ssDNA-dsDNA junction in the 4-nucleotide overhang shifts further away from the catalytic triad and positions itself onto the Val110 side chain of an adjacent α-

helical shelf instead of base-stacking with the Trp81 side chain observed in the structure with the 3-nucleotide overhang (Figures 6C, 6D).

Overall, the structure demonstrates the ability of HMCES to interact with DNA overhangs of different lengths, which are expected to be present at switch regions following strand resection (Figures 6B, 6C, 6D). By binding to the 3' hydroxyl end of short overhangs, HMCES is assumed to protect the ends from further resection while at the same time presenting the bases of these short sequences for recognition in subsequent steps of repair. Co-incubation of 5' DNA overhangs with recombinant HMCES SRAPd protected against Exonuclease III (Exo III) activity in a concentration-dependent manner, suggesting that HMCES could potentially function to control excessive processing of DNA DSBs generated by exonucleases at switch regions (Figure 6E). A key common feature of 3' overhang recognition is the alignment of the 3' hydroxyl with the absolutely conserved catalytic triad through hydrogen bonding with H210. Given that mutation of the catalytic C2A did not alter the ability of HMCES to mediate CSR, this suggests that the H210 residue may have acquired a new "moonlighting" activity, at least in jawed vertebrates – to possibly align 3' overhangs for Alt-EJ.

Discussion

Activated B cells undergo two essential processes of genome editing in immunoglobulin gene loci – somatic hypermutation which occurs in Ig variable regions and underlies selection for increased antigen affinity, and class switch recombination which alters antibody isotypes from IgM/ IgD to the more potent immune effector isotypes (IgG, IgA and IgE). While somatic hypermutation generates cytidine to uridine mutations on a single DNA strand that are repaired by abundant U:G mismatch repair enzymes such as UNG and SMUG, class switch recombination involves double-strand DNA breaks (DNA DSBs) that are potentially far more dangerous in terms of genome integrity. The DNA DSBs generated during CSR are repaired by one of two redundant mechanisms: the well-characterized c-NHEJ pathway which promotes joins with no or minimal microhomologies, or the less well-understood microhomology-dependent Alt-EJ pathway(Alt et al., 2013; Bennardo et al., 2008; Chang et al., 2017; Frit et al., 2014; Stavnezer and Schrader, 2014) (Figure 6F). Since the Alt-EJ pathway operates with much slower kinetics than the c-NHEJ pathway during CSR (Han and Yu, 2008), HMCES-deficient primary B cells and CH12 cells showed defects in switching to most Ig isotypes (IgG1, IgA, IgE) at later time-points of stimulation. Among the different isotypes analyzed here, switching to IgA was most strongly affected by HMCES deficiency, likely due to the relatively slower kinetics of switching to IgA and the more extensive sequence homologies observed between Sμ and Sα regions. The lack of obvious defects in switching to IgG3 and IgG2b isotypes in HMCES-deficient B cells could reflect faster kinetics of switching to these isotypes and hence, lesser dependence on the Alt-EJ pathway. Taken together, our studies show that HMCES, a protein already reported to be involved in protecting stalled replication forks against error prone DNA repair(Mohni et al., 2019), also plays an important and specific role in the Alt-EJ pathway of class switch recombination in activated murine B cells.

How does the reported role of HMCES as an oxidized methylcytosine (oxi-mC) binding protein relate to its potential role in DNA repair, in the context of abasic site repair as well as Alt-EJ? TET proteins were shown to deposit 5hmC at DNA DSBs in HeLa cells(Kafer et al., 2016), but this study did not demonstrate a functional role for TET and 5hmC in DNA repair. Future studies will be required to TET activity plays a role in the recruitment of HMCES to sites of DNA damage. In our own studies, loss of HMCES did not cause changes in 5hmC, nor did it lead to major alterations in the hematopoietic compartment, where TET proteins and the oxi-mC marks that they catalyze are known to have important functions (Cimmino et al., 2011; Lio and Rao, 2019; Pastor et al., 2013). Even though we have not formally ruled out the possibility for a more specific role of HMCES in recognition of the other two oxi-mC bases, 5-formylcytosine (5fC) and 5-carboxylcytosine (5caC), our results clearly show that HMCES is dispensable for major lineage commitment decisions during hematopoiesis that are influenced by the activities of TET enzymes.

The molecular mechanisms that underlie repair of DNA DSBs by the Alt-EJ pathway during CSR and in other cellular contexts remains poorly understood. The Alt-EJ pathway requires the concerted nuclease action of CTIP and the MRE11-RAD50-NBS1 (MRN) complex to carry out DNA end resection (Figure 6F)(Lee-Theilen et al., 2011). During CSR, Alt-EJ requires RAD52 binding to DSBs, PARP1 activity and recruitment of the MRN complex (Chang et al., 2017; Lee-Theilen et al., 2011; Robert et al., 2009; Zan et al., 2017). The MRN complex processes the DNA DSBs generated during CSR to generate 5’ overhangs through its 3’ to 5’ exonuclease activity (Chang et al., 2017; Liu and Huang, 2016). In the presence of CTIP, however, the MRN complex exhibits an endonuclease activity that introduces a nick in the DNA, following which the 3’ to 5’ exonuclease activity of MRN complex can potentially create 3’ overhangs(Anand et al., 2016; Chang et al., 2017; Liu and Huang, 2016). Yet, how these ssDNA overhangs generated after initial end processing are brought together and eventually ligated by LIGASE1 and LIGASE3(Masani et al., 2016) during Alt-EJ is unclear. Our studies identify HMCES as an important downstream factor in the Alt-EJ pathway that mediates DNA DSB repair (Figure 6F). Since the microhomology-mediated pathway is utilized for DNA DSB repair at collapsed replication forks(Truong et al., 2013), we speculate that HMCES may also operate via similar mechanisms to maintain replication fork stability.

Our previously reported structures of SRAPd(Halabelian et al., 2019) showed how HMCES could bind DNA molecules containing both 3’ and 5’ overhangs. The SRAPd_P5nt presented here demonstrates that the ssDNA-dsDNA junction of the 3’ overhang DNA can move at least one nucleotide further away from the catalytic site, to accommodate binding of a longer four ssDNA overhang sequence. In this structure, the dsDNA makes no specific contacts with SRAPd, a mode of binding which may be relevant in the Alt-EJ pathway of CSR, which would require the interaction of HMCES with variable, longer ssDNA overhangs (Figures 6B, 6C, 6D). A recent study resolved the crystal structure of prokaryotic YedK protein in complex with a ssDNA heptamer containing an abasic site (Thompson et al., 2019). Similar to our HMCES structures presented here and published previously, prokaryotic YedK cradles the phosphoribosyl backbone of ssDNA into a positively charged channel containing both R77 and R162 (cognates of R98 and R212 of human HMCES (Thompson et al., 2019), but flips its abasic site into the catalytic triad pocket to crosslink

with Cys2 (Figure S7A). The inability of HMCES R212A mutant to rescue the defect in CSR in our studies strongly argues that ssDNA binding activity of HMCES is required for its role in Alt-EJ directed CSR. The HMCES C2A mutant which lacks the autoproteolytic and covalent crosslinking activity at abasic sites is still able to rescue the defect in CSR, likely because it retains the ability to bind both 5' and 3' ssDNA overhangs, as shown previously(Halabelian et al., 2019; Mohni et al., 2019). We put forth a model in which the ability of HMCES to bind 3' and 5' overhangs(Halabelian et al., 2019; Mohni et al., 2019) may allow HMCES to engage resected DNA ends in a manner that makes them amenable to strand annealing during microhomology-directed joins while protecting them against extensive, unwanted processing by exonucleases (Figure 6F). In support of our model, we note that a recent study resolved structure of two prokaryotic YedK molecules in complex with two ssDNAs, such that the 3' complementary ends protrude out and extend to anneal with each other (Figures S7B, S7C) (PDB ID: 6KBS) (Wang et al., 2019). This conformation is likely biologically relevant, since it resembles the structure expected to form at HMCES-mediated, microhomology-directed DNA end joins during CSR.

In summary, we propose that the ssDNA-binding pockets of HMCES are flexible and can accommodate DNA molecules in distinct configurations, several of which may be present during the formation of DNA DSB joins in CSR. Our studies identify novel functions of HMCES in regulating a non-canonical DNA end joining pathway that relies on microhomologies to mend DNA ends. Notably, in diverse bacteria the SRAP genes are part of mobile operons along with genes coding for the orthologs of Ku and the ATP-dependent ligase(Aravind et al., 2013; Krishna and Aravind, 2010). This suggests that the complementary role played by the two specialized DNA-binding modules Ku and SRAP in different pathways of end-joining during DNA repair likely had ancient antecedents in the prokaryotic world. Our current work shows how these two repair mechanisms have been recruited together in eukaryotes to mediate DNA repair in a directed double strand-break repair mechanism, namely CSR.

STAR Methods

Lead Contact and Material Availability

Further information and requests for resources and reagents should be directed to and will be fulfilled by lead contact, Anjana Rao (arao@lji.org). All reagents generated in the study will be made available upon request to the lead contact but may require a completed Materials Transfer Agreement if there is potential for commercial application.

Experimental Models and Subject details

Mice.—*Hmces*-deficient mice were generated as previously described(Kweon et al., 2017) and maintained on a C57BL/6J genetic background for at least 6 generations. All mice used in the studies here were 8–16 weeks of age and were housed in specific-pathogen free animal facility at the La Jolla Institute for Immunology. Both male and female mice were used in the studies. All procedures were performed according to protocols approved by the Institutional Animal Care and Use Committee.

Cell lines and primary cell cultures.—CH12F3 (CH12) cells and primary B cells were cultured in RPMI 1640 media supplemented with 10% FBS, 1× MEM non-essential amino acids, 10mM HEPES, 2mM Glutamax, 1mM sodium pyruvate, 55μM 2-mercaptoethanol and penicillin and streptomycin (all from Life technologies). U2OS reporter cell lines (EJ2 and EJ5) were cultured in DMEM/F12 media supplemented with 10% FBS, 1× MEM non-essential amino acids, 10mM HEPES, 2mM Glutamax, 55μM 2-mercaptoethanol and penicillin and streptomycin (all from Life technologies).

Method details

Immunization.—For 4-hydroxy-3-nitrophenylacetyl-conjugated ovalbumin (NP-OVA; Biosearch) immunization, the hapten-conjugated protein was diluted to 1 mg/mL in PBS was mixed with 1 volume of Alhydrogel (Invivogen) and injected into hind footpads (10 μg in 20 μL per injection). Germinal center response was analyzed 7 days post-injections and the two draining popliteal lymph nodes were pooled for analysis. Hapten-specific B cells were identified by positive staining with NP-phycoerythrin (BioSearch Technologies).

B cell isolation and class switch recombination (CSR).—B cells were isolated with the EasySep Mouse B cell isolation kit (Stem Cell Technology, Canada) from total splenocytes. To induce CSR from IgM to IgG1 or IgE, B cells (5×10^5–1×10^6 cells/ mL) were activated with 1 μg/mL anti-CD40 clone 1C10, Biolegend) and rmIL-4 (10 ng/mL, Peprotech). For IgG3 and IgG2b switching, B cells were activated with 25 ug/mL of LPS from *E. coli* O55:B5 (Sigma, St. Louis, MO) and 10 ng/mL rmIL-4 at 37°C 5% CO 2. For IgA and IgG1 switching, B cells were activated with anti-CD40 (1 μg/mL, clone 1C10, Biolegend), rmIL-4 (10 ng/mL, Peprotech), rmIL-5 (10ng/mL, Peprotech), and rhTGFβ (1 ng/mL).

CSR stimulation in CH12 cells.—For CSR from IgM to IgA in CH12 cell line, cells were plated at a density of $50X10^3$ per mL of media and stimulated with anti-CD40 (1 μg/mL, clone 1C10, Biolegend), rmIL-4 (10 ng/mL, Peprotech), and rhTGFβ (1 ng/mL) (CIT) for 72 hours or the indicated time-points.

CRISPR-Cas9 mediated gene targeting.—Specific guide RNAs (gRNA) (Table 2) for CRISPR mediated targeting were cloned into pX330 vector with a GFP reporter digested with BbsI restriction enzyme. For *Hmces and Lig4* gene targeting in CH12 cells, 250 ng of two pX330 vectors with different gRNA were transiently transfected in CH12 cells plated at a density of $2X10^5$ cells/ml of media using the Neon transfection system with 2 pulses of 1150V for 30ms in a 10ul volume. 24 hours post-transfection the GFP positive cells were purified by flow cytometry and plated at single cell density for 7–10 days. Individual clones derived from single cells were genotyped to confirm the desired deletion. For U2OS reporter lines, 250 ng of two pX330 vectors containing different gRNA were transiently transfected using the Jet Prime transfection reagent (Polyplus) according to manufacturer's instructions. 24 hours post-transfection, cells were trypsinized and plated at single cell density. DNA from single cell clones was isolated 14–17 days post initial plating and genotyping was performed to test for desired deletion. Disruptions of open reading frames for each clone

were confirmed by Immunoblotting as described below. Oligonucleotides for gRNAs and primers for genotyping are listed in Key resource table.

Lentiviral transduction of CH12 cells.—Lentivirus were produced by transfecting 293T cells with pLKO lentiviral vectors (5μg), and pMD2G (1.25μg) and psPax2 (3.75μg) packaging vectors. The lentiviral supernatants were added to CH12 cells plated at a density of $50X10^3$ per mL of media and centrifuged at 2,000 rpm at >20°C for two hours. For lentiviral vectors harboring GFP reporters (HMCES mutant constructs) the transduced cells were either analyzed based on Flow Cytometry while gating on GFP+ cells or were purified by flow cytometry assisted cell sorting. For lentiviral vectors containing puromycin resistance markers (shRNA vectors), transduced cells were selected starting at 48 hours post-transduction with 2μg/ml puromycin for at least 72 hours. The shRNA vectors against KU70, CTIP and a non-targeting mammalian shRNA control vector were obtained from Sigma mission libraries.

Analysis of Switch Junctions.—For Sμ-Sα junctional analysis, 100 ng of genomic DNA isolated from CH12 stimulated with CIT for 72 hours was PCR amplified with primers described in supplementary table 2 using the Phusion polymerase system (Invitrogen). The PCR conditions were 98 C for 3 minutes; 98C 30 seconds, 60C 30 seconds and 72C for 2 minutes for a total of 38 cycles. The PCR products 1–2 kilobases long were gel purified and cloned using the Zero blunt topo cloning system (Invitrogen). For Sμ-Sγ1 junctional analysis, 100 ng of genomic DNA isolated from *Hmces*$^{+/+}$ and *Hmces*$^{-/-}$ primary B cells stimulated with anti-CD40 and IL-4 for 4 days was PCR amplified with primers described supplementary table 2 using the Phusion polymerase system (Invitrogen). The PCR conditions were 98 C for 3 minutes; 98C 30 seconds, 58C 30 seconds and 72C for 2 minutes for a total of 35 cycles. The PCR products were purified and cloned using Zero blunt topo cloning system (Invitrogen). DNA from individual bacterial colonies were sequenced using Sanger sequencing (MCLAB) and aligned to switch-mu (MUSIGCD07), switch-alpha sequence (MUSIALPHA) and switch gamma 1 (MUSIGHANB) using Mac Vector software.

DNA repair assays in U2OS reporter cells.—The U2OS reporter cell were transiently co-transfected with pCBA I-SCEI vector and a reporter vector expressing Thy1.1 using the Jet Prime system (Polyplus). 48 hours post transfection transfected cells were gated based on Thy1.1 expression using flow cytometry and the frequency of GFP+ cells were determined.

Flow cytometry.—Cells were stained in FACS buffer (0.5% bovine serum albumin, 2mM EDTA, and 0.05% sodium azide in PBS) with indicated antibodies for 30 mins on ice. Cells were washed and then fixed with 1% paraformaldehyde (diluted from 4% with PBS; Affymetrix) before FACS analysis using FACS Celesta and FACS LSR II (BD Biosciences). Antibodies and dye were from BioLegend, Southern Biotech and BD Pharmingen. Data were analyzed with FlowJo (FlowJo LLC, Ashland, OR).

Immunoblotting.—Proteins isolated from B cells with RIPA buffer were resolved using NuPAGE 4–12% Bis-Tris gel (ThermoFisher) and transferred from gel to PVDF membrane using Wet/Tank Blotting Systems (Bio-Rad). Membrane was blocked with 5% non-fat milk (Bob's red mill) in TBSTE buffer (50mM Tris-HCl pH 7.4, 150mM NaCl, 0.05% Tween-20,

1mM EDTA), incubated with indicated primary antibodies, followed by secondary antibodies conjugated with horseradish peroxidase (HRP) and signal was detected with enhanced chemiluminescence reagents (Invitrogen) and X-ray film. Antibodies against HMCES (clone B2), KU70 (clone E5), CTIP (clone D4) and LIGASE4 (clone D8) were purchased from Santa Cruz Biotechnology. Anti-HMCES antibody recognizes an epitope between amino acids 111–153 of human HMCES which is also identical in sequence to mouse HMCES.

RNA extraction, cDNA synthesis, and quantitative RT-PCR.—Total RNA was isolated with RNeasy plus kit (Qiagen, Germany) or with Trizol (ThermoFisher, Waltham, MA) following manufacturer's instructions. cDNA was synthesized using SuperScript III reverse transcriptase (ThermoFisher) and quantitative RT-PCR was performed using FastStart Universal SYBR Green Master mix (Roche, Germany) on a StepOnePlus real-time PCR system (ThermoFisher). Gene expression was normalized to *Gapdh*. Primers are listed in Supplementary Table 2.

DNA dot blot.—To analyze 5hmC abundance, genomic DNA was treated with sodium bisulfite using the Methylcode Bisulite conversion kit (Invitrogen) as per the manufacturer's instructions. DNA was diluted two-fold serially with TE buffer, denatured in 0.4 M sodium hydroxide and 10 mM EDTA at 95°C for 10 minutes, an d then immediately chilled on ice. Equally volume of ice-cold 2M ammonium acetate pH 7.0 was added and incubated on ice for 10 minutes. Denatured DNA were spotted on a nitrocellulose membrane using a Bio-Dot apparatus (Bio-Rad), washed with 2× SSC buffer (300 mM NaCl and 30 mM sodium citrate), and baked in a vacuum oven at 80°C for 2 hours. To detect CMS, mem brane was rehydrated with TBSTE buffer and blocked with 5% non-fat milk (Bob's red mill) in TBSTE buffer. CMS was detected with primary rabbit anti-CMS antisera (in house) following the procedures above for Immunoblotting.

Chromatin Immunoprecipitation and quantitative PCR (ChIP-qPCR).—Chromatin immunoprecipitation was performed as described before. Briefly, cells were fixed with 1% formaldehyde (ThermoFisher) at room temperature for 10 mins at 1×10^6 cell/mL in media, quenched with 125 mM glycine, washed twice with ice cold PBS. Cells were pelleted, snap-frozen with liquid nitrogen and store at −80°C until use. To isolate nu clei for sonication, cell pellets were thawed on ice and lysed with lysis buffer (50 mM HEPES pH 7.5, 140 mM NaCl, 1mM EDTA, 10% glycerol, 0.5% NP40, 0.25% Triton-X100) for 10 mins at 4°C with rotation, washed once wi th washing buffer (10 mM Tris-HCl pH 8.0, 200 mM NaCl, 1 mM EDTA, 0.5 mM EGTA) and twice with shearing buffer (10 mM Tris-HCl pH 8.0, 1 mM EDTA, 0.1% SDS). Nuclei were resuspended in 1mL shearing buffer and sonicated with Covaris E220 using 1 mL milliTUBE (Covaris, Woburn, MA) for 18–20 minutes (Duty Cycle 5%, intensity 140 Watts, cycles per burst 200). After sonication, insoluble debris was removed by centrifugation at 20,000 × *g*. Buffer for chromatin was adjusted with 1 volume of 2× conversion buffer (10 mM Tris-HCl pH 7.5, 280 mM NaCl, 1 mM EDTA, 1mM EGTA, 0.2% sodium deoxycholate, 0.2% Triton-X100, 1% Halt protease inhibitors with 0.1% SDS. Chromatin was pre-cleared with washed protein G dynabeads (ThermoFisher) for 2 hours, incubated with antibodies and protein A dynabeads overnight

(all procedures were at 4°C with ro tation). The bead-bound chromatin was washed three times with RIPA buffer (50 mM Tris-HCl pH 8.0, 150 mM NaCl, 1 mM EDTA, 0.5% sodium deoxycholate, 1% NP-40, 0.1% SDS), and once with TE (10 mM Tris-HCl pH 8.0, 1 mM EDTA). Chromatin was eluted from beads with elution buffer (100 mM $NaHCO_3$, 1% SDS,) following digestion with 1mg/ml RnaseA (Qiagen) for 37 minutes at 37°C with constant shaking. NaCl and proteinas e K (Ambion) were added to the RnaseA digested chromatin at concentrations of 250 mM and 0.5 mg/mL, respectively, and de-crosslinked at 65°C overnight with constant shaking. DNA was purified with Zymo ChIP DNA Clean & Concentrator-Capped Column (Zymo Research, Irvine, CA). Primers for ChIP qPCR are listed in Supplementary Table 2

Protein Expression, Purification, Crystallization and Structural Determination

Human HMCES SRAPd was expressed and purified as described before (Halabelian et al., 2019). A thirteen nucleotide palindromic DNA (5'-CAACGTTGTTTTT-3') (ordered from IDT DNA) was annealed by incubating the sample at 95°C for ten minutes, then transferri ng it into boiled water and letting it to gradually cool down at room temperature. SRAPd at 10 mg/mL was mixed with palindromic dsDNA at 1:1.2 ratio and incubated at room temperature for 30 minutes before setting crystallization plates. Diffraction quality crystals were obtained in 96 well sitting drop containing 11% (w/v) PEG 8K, 0.1M $CaCl_2$, 0.1M Hepes pH 7.5 as precipitant solution. Crystals were soaked in precipitant solution supplemented with 20% Glycerol and cryo-cooled in liquidnitrogen.

SRAPd_P5nt diffraction data was collected at the 5.0.1 beamline of the Advanced Light Source (ALS) Berkeley Lab. XDS(Kabsch, 2010) and Aimless (Evans and Murshudov, 2013; Winn et al., 2011) were used to process and merge the dataset, respectively. SRAPd_P5nt initial phases were obtained by using Apo SRAPd of HMCES (PDB ID: 5KO9) as initial model in molecular replacement using Phaser-MR(McCoy et al., 2007). COOT(Emsley et al., 2010) was used to manually build the DNA, then refined with refmac5(Steiner et al., 2003). The final model was validated by Molprobity(Williams et al., 2018). PyMOL (http://pymol.org) was used to generate the figures. Data collection and refinement statistics are shown in (Supplementary Table 3).

DNA-overhang end exonuclease protection assay.—A fluorescein tagged DNA having 6-nucleotide overhang at its 5' end was used in Exonuclease III protection assay with Human HMCES SRAPd. The DNA overhang was annealed by mixing equimolar amounts of DNA-A and DNA-B in boiled water and gradually cooled down at room temperature. DNA-A: 5'-TCGGATTCTTCTGGTCCGGATGGTAGTTAAGT*G*T*T*G*A*G-3', DNA-B: 5'-/6FAM/-C*T*C*A*A*C*ACTTAACTACCATCCGGACCAGAAGA-3' (6FAM represents 5-Carboxyfluorescein). Both DNA oligos contain 6 phosphorothioate linkages at its blunt end (highlighted in asterisk) in order to restrict the Exonuclease III degradation from the fluorescein labeled end. A 20 μL final volume was used for each reaction mixture containing 1μM fluorescein tagged DNA, 66 mM Tris-HCl (pH 8.0 at 30 °C), 0.66 mM MgCl 2, 2units of Exonuclease III (purchased from ThermoFisher, catalog Number: EN0191) and increasing concentrations of purified Human HMCES SRAPd (as described previously) (Halabelian et al., 2019). The reaction mixture was first incubated at 37°C for 30

minutes. Then, the reaction was stopped by adding Proteinase-K (0.18 mg/mL) and 10 mM ethylenediaminetetraacetic acid (EDTA) and incubated at 58°C for 1 2 minutes. DNA-loading dye (purchased from ThermoFisher, catalog Number: R0611) was added to the reaction mixture and loaded into Tris-Borate-EDTA (TBE) 15% polyacrylamide gel and run at 160V for 40 minutes in 0.5% TBE running buffer. Bands were visualized by FAM fluorescence.

Data and Code availability

Original scanned image files for western blots in the paper is available at Mendeley data, (DOI: 10.17632/k784xkjg9k.2). Co-crystal structure of HMCES SRAPd in complex with ssDNA has been deposited in Protein database (PDB), PDB ID:6OOV.

Quantification and Statistical Analysis

Statistical analyses and bar plots were performed and plotted with Prism 7. Bar graphs indicate mean +/− standard deviations. The statistical tests used to determine significance are mentioned in the figure legends of the corresponding figures.

Supplementary Material

Refer to Web version on PubMed Central for supplementary material.

Acknowledgements

We would like to thank Dr. J. Stark for providing the c-NHEJ and Alt-EJ U2OS reporter cell lines; and C. Kim, L. Nosworthy, D. Hinz, and C. Dillingham (LJI Flow Cytometry Core) for help with cell sorting. BD FACSAria II is supported by NIH (NIH S10OD016262, NIH S10RR027366). We thank Dr. H. Wyatt for the recommendations on the exonuclease protection assay. This research used resources of the Advanced Light Source, which is a DOE Office of Science User Facility under contract no. DE-AC02-05CH11231. V.S. is supported by Leukemia and Lymphoma Society Postdoctoral Fellowship (grant ID: 5463-18). D.S.C. is supported by CONACYT/UCMEXUS Fellowship. The Structural Genomics Consortium is a registered charity (no: 1097737) that receives funds from AbbVie; Bayer Pharma AG; Boehringer Ingelheim; Canada Foundation for Innovation; Eshelman Institute for Innovation; Genome Canada through Ontario Genomics Institute [OGI-055]; Innovative Medicines Initiative (EU/EFPIA) [ULTRA-DD: 115766]; Janssen, Merck & Co.; Novartis Pharma AG; Ontario Ministry of Research Innovation and Science (MRIS); Pfizer, São Paulo Research Foundation-FAPESP, Takeda and the Wellcome Trust. This work is supported by the Canadian Institutes of Health Research (FDN154328) and Natural Sciences and Engineering Research Council (no. RGPIN-2015-05939) to C.H.A., National Institutes of Health (NIH) grants R35 CA210043 and R01 AI109842 to A.R., and intramural funds of the National Library of Medicine, NIH, USA, to L.A.

References

Alt FW, Zhang Y, Meng FL, Guo C, and Schwer B (2013). Mechanisms of programmed DNA lesions and genomic instability in the immune system. Cell 152, 417–429. [PubMed: 23374339]

Anand R, Ranjha L, Cannavo E, and Cejka P (2016). Phosphorylated CtIP Functions as a Co-factor of the MRE11-RAD50-NBS1 Endonuclease in DNA End Resection. Mol Cell 64, 940–950. [PubMed: 27889449]

Aravind L, Anand S, and Iyer LM (2013). Novel autoproteolytic and DNA-damage sensing components in the bacterial SOS response and oxidized methylcytosine-induced eukaryotic DNA demethylation systems. Biol Direct 8, 20. [PubMed: 23945014]

Bennardo N, Cheng A, Huang N, and Stark JM (2008). Alternative-NHEJ is a mechanistically distinct pathway of mammalian chromosome break repair. PLoS Genet 4, e1000110. [PubMed: 18584027]

Boboila C, Yan C, Wesemann DR, Jankovic M, Wang JH, Manis J, Nussenzweig A, Nussenzweig M, and Alt FW (2010). Alternative end-joining catalyzes class switch recombination in the absence of both Ku70 and DNA ligase 4. J Exp Med 207, 417–427. [PubMed: 20142431]

Boehm EM, and Washington MT (2016). R.I.P. to the PIP: PCNA-binding motif no longer considered specific: PIP motifs and other related sequences are not distinct entities and can bind multiple proteins involved in genome maintenance. Bioessays 38, 1117–1122. [PubMed: 27539869]

Chang HHY, Pannunzio NR, Adachi N, and Lieber MR (2017). Non-homologous DNA end joining and alternative pathways to double-strand break repair. Nat Rev Mol Cell Biol 18, 495–506. [PubMed: 28512351]

Cimmino L, Abdel-Wahab O, Levine RL, and Aifantis I (2011). TET family proteins and their role in stem cell differentiation and transformation. Cell Stem Cell 9, 193–204. [PubMed: 21885017]

Emsley P, Lohkamp B, Scott WG, and Cowtan K (2010). Features and development of Coot. Acta Crystallogr D Biol Crystallogr 66, 486–501. [PubMed: 20383002]

Evans PR, and Murshudov GN (2013). How good are my data and what is the resolution? Acta Crystallogr D Biol Crystallogr 69, 1204–1214. [PubMed: 23793146]

Frit P, Barboule N, Yuan Y, Gomez D, and Calsou P (2014). Alternative end-joining pathway(s): bricolage at DNA breaks. DNA Repair (Amst) 17, 81–97. [PubMed: 24613763]

Gunn A, and Stark JM (2012). I-SceI-based assays to examine distinct repair outcomes of mammalian chromosomal double strand breaks. Methods Mol Biol 920, 379–391. [PubMed: 22941618]

Halabelian L, Ravichandran M, Li Y, Zeng H, Rao A, Aravind L, and Arrowsmith CH (2019). Structural basis of HMCES interactions with abasic DNA and multivalent substrate recognition. Nat Struct Mol Biol 26, 607–612. [PubMed: 31235913]

Han L, and Yu K (2008). Altered kinetics of nonhomologous end joining and class switch recombination in ligase IV-deficient B cells. J Exp Med 205, 2745–2753. [PubMed: 19001141]

Howard SM, Yanez DA, and Stark JM (2015). DNA damage response factors from diverse pathways, including DNA crosslink repair, mediate alternative end joining. PLoS Genet 11, e1004943. [PubMed: 25629353]

Huang Y, Pastor WA, Zepeda-Martinez JA, and Rao A (2012). The anti-CMS technique for genome-wide mapping of 5-hydroxymethylcytosine. Nat Protoc 7, 1897–1908. [PubMed: 23018193]

Ito S, Shen L, Dai Q, Wu SC, Collins LB, Swenberg JA, He C, and Zhang Y (2011). Tet proteins can convert 5-methylcytosine to 5-formylcytosine and 5-carboxylcytosine. Science 333, 1300–1303. [PubMed: 21778364]

Iyer LM, Tahiliani M, Rao A, and Aravind L (2009). Prediction of novel families of enzymes involved in oxidative and other complex modifications of bases in nucleic acids. Cell Cycle 8, 1698–1710. [PubMed: 19411852]

Kabsch W (2010). Xds. Acta Crystallogr D Biol Crystallogr 66, 125–132. [PubMed: 20124692]

Kafer GR, Li X, Horii T, Suetake I, Tajima S, Hatada I, and Carlton PM (2016). 5-Hydroxymethylcytosine Marks Sites of DNA Damage and Promotes Genome Stability. Cell Rep 14, 1283–1292. [PubMed: 26854228]

Ko M, Huang Y, Jankowska AM, Pape UJ, Tahiliani M, Bandukwala HS, An J, Lamperti ED, Koh KP, Ganetzky R, et al. (2010). Impaired hydroxylation of 5-methylcytosine in myeloid cancers with mutant TET2. Nature 468, 839–843. [PubMed: 21057493]

Krishna SS, and Aravind L (2010). The bridge-region of the Ku superfamily is an atypical zinc ribbon domain. J Struct Biol 172, 294–299. [PubMed: 20580930]

Kweon SM, Zhu B, Chen Y, Aravind L, Xu SY, and Feldman DE (2017). Erasure of Tet-Oxidized 5-Methylcytosine by a SRAP Nuclease. Cell Rep 21, 482–494. [PubMed: 29020633]

Lee-Theilen M, Matthews AJ, Kelly D, Zheng S, and Chaudhuri J (2011). CtIP promotes microhomology-mediated alternative end joining during class-switch recombination. Nat Struct Mol Biol 18, 75–79. [PubMed: 21131982]

Lio CJ, and Rao A (2019). TET Enzymes and 5hmC in Adaptive and Innate Immune Systems. Front Immunol 10, 210. [PubMed: 30809228]

Liu T, and Huang J (2016). DNA End Resection: Facts and Mechanisms. Genomics Proteomics Bioinformatics 14, 126–130. [PubMed: 27240470]

Masani S, Han L, Meek K, and Yu K (2016). Redundant function of DNA ligase 1 and 3 in alternative end-joining during immunoglobulin class switch recombination. Proc Natl Acad Sci U S A 113, 1261–1266. [PubMed: 26787901]

McCoy AJ, Grosse-Kunstleve RW, Adams PD, Winn MD, Storoni LC, and Read RJ (2007). Phaser crystallographic software. J Appl Crystallogr 40, 658–674. [PubMed: 19461840]

Mohni KN, Wessel SR, Zhao R, Wojciechowski AC, Luzwick JW, Layden H, Eichman BF, Thompson PS, Mehta KPM, and Cortez D (2019). HMCES Maintains Genome Integrity by Shielding Abasic Sites in Single-Strand DNA. Cell 176, 144–153 e113. [PubMed: 30554877]

Nakamura M, Kondo S, Sugai M, Nazarea M, Imamura S, and Honjo T (1996). High frequency class switching of an IgM+ B lymphoma clone CH12F3 to IgA+ cells. Int Immunol 8, 193–201. [PubMed: 8671604]

Pastor WA, Aravind L, and Rao A (2013). TETonic shift: biological roles of TET proteins in DNA demethylation and transcription. Nat Rev Mol Cell Biol 14, 341–356. [PubMed: 23698584]

Robert I, Dantzer F, and Reina-San-Martin B (2009). Parp1 facilitates alternative NHEJ, whereas Parp2 suppresses IgH/c-myc translocations during immunoglobulin class switch recombination. J Exp Med 206, 1047–1056. [PubMed: 19364882]

Spruijt CG, Gnerlich F, Smits AH, Pfaffeneder T, Jansen PW, Bauer C, Munzel M, Wagner M, Muller M, Khan F, et al. (2013). Dynamic readers for 5-(hydroxy)methylcytosine and its oxidized derivatives. Cell 152, 1146–1159. [PubMed: 23434322]

Stavnezer J, and Schrader CE (2014). IgH chain class switch recombination: mechanism and regulation. J Immunol 193, 5370–5378. [PubMed: 25411432]

Steiner RA, Lebedev AA, and Murshudov GN (2003). Fisher's information in maximum-likelihood macromolecular crystallographic refinement. Acta Crystallogr D Biol Crystallogr 59, 2114–2124. [PubMed: 14646069]

Tahiliani M, Koh KP, Shen Y, Pastor WA, Bandukwala H, Brudno Y, Agarwal S, Iyer LM, Liu DR, Aravind L, et al. (2009). Conversion of 5-methylcytosine to 5-hydroxymethylcytosine in mammalian DNA by MLL partner TET1. Science 324, 930–935. [PubMed: 19372391]

Thompson PS, Amidon KM, Mohni KN, Cortez D, and Eichman BF (2019). Protection of abasic sites during DNA replication by a stable thiazolidine protein-DNA cross-link. Nat Struct Mol Biol 26, 613–618. [PubMed: 31235915]

Truong LN, Li Y, Shi LZ, Hwang PY, He J, Wang H, Razavian N, Berns MW, and Wu X (2013). Microhomology-mediated End Joining and Homologous Recombination share the initial end resection step to repair DNA double-strand breaks in mammalian cells. Proc Natl Acad Sci U S A 110, 7720–7725. [PubMed: 23610439]

Wang N, Bao H, Chen L, Liu Y, Li Y, Wu B, and Huang H (2019). Molecular basis of abasic site sensing in single-stranded DNA by the SRAP domain of E. coli yedK. Nucleic Acids Res.

Williams CJ, Headd JJ, Moriarty NW, Prisant MG, Videau LL, Deis LN, Verma V, Keedy DA, Hintze BJ, Chen VB, et al. (2018). MolProbity: More and better reference data for improved all-atom structure validation. Protein Sci 27, 293–315. [PubMed: 29067766]

Winn MD, Ballard CC, Cowtan KD, Dodson EJ, Emsley P, Evans PR, Keegan RM, Krissinel EB, Leslie AG, McCoy A, et al. (2011). Overview of the CCP4 suite and current developments. Acta Crystallogr D Biol Crystallogr 67, 235–242. [PubMed: 21460441]

Xu Z, Fulop Z, Zhong Y, Evinger AJ 3rd, Zan H, and Casali P (2005). DNA lesions and repair in immunoglobulin class switch recombination and somatic hypermutation. Ann N Y Acad Sci 1050, 146–162. [PubMed: 16014529]

Yan CT, Boboila C, Souza EK, Franco S, Hickernell TR, Murphy M, Gumaste S, Geyer M, Zarrin AA, Manis JP, et al. (2007). IgH class switching and translocations use a robust non-classical end-joining pathway. Nature 449, 478–482. [PubMed: 17713479]

Zan H, Tat C, Qiu Z, Taylor JR, Guerrero JA, Shen T, and Casali P (2017). Rad52 competes with Ku70/Ku86 for binding to S-region DSB ends to modulate antibody class-switch DNA recombination. Nat Commun 8, 14244. [PubMed: 28176781]

Highlights:

- HMCES is dispensable for normal hematopoiesis in mice.
- HMCES deficiency causes a defect in Class Switch Recombination (CSR) of B cells.
- HMCES functions in the Alt-EJ pathway of the DNA DSB repair to regulate CSR.
- HMCES binds and protects ssDNA overhangs to promote Alt-EJ pathway.

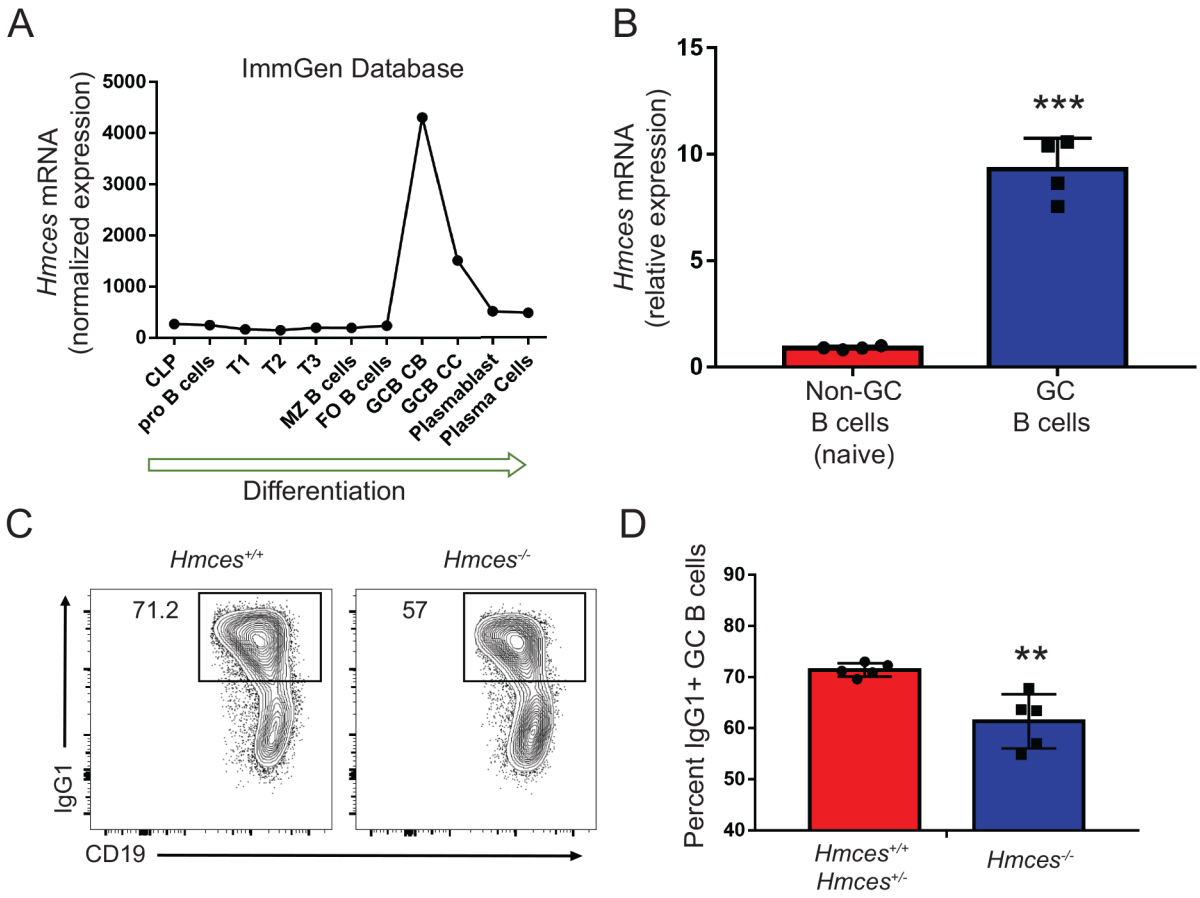

Figure 1: HMCES deficiency leads to a significant defect in CSR in germinal center B cells.

A) Normalized expression of *Hmces* mRNA in different B cell subsets (data from the Immgen database-www.immgen.org). **B)** Relative mRNA expression of *Hmces* measured by qRT-PCR in sorted GC B cells and naïve non-GC B cells from mice immunized with Sheep Red Blood Cells (SRBCs). **C)** Flow cytometry plots showing class switch recombination (CSR) from IgM to IgG1 in GC B cells from $Hmces^{+/+}$ and $Hmces^{-/-}$ mice. **D)** Bar graphs quantifying the frequencies of $IgG1^{+}$ GC B cells from $Hmces^{+/+}$ and $Hmces^{-/-}$ mice. Data are represented as mean ± SD. Each dot represents a mouse. Statistical significance was calculated using student t-test. ***p value ≤0.001, **p value ≤0.005.

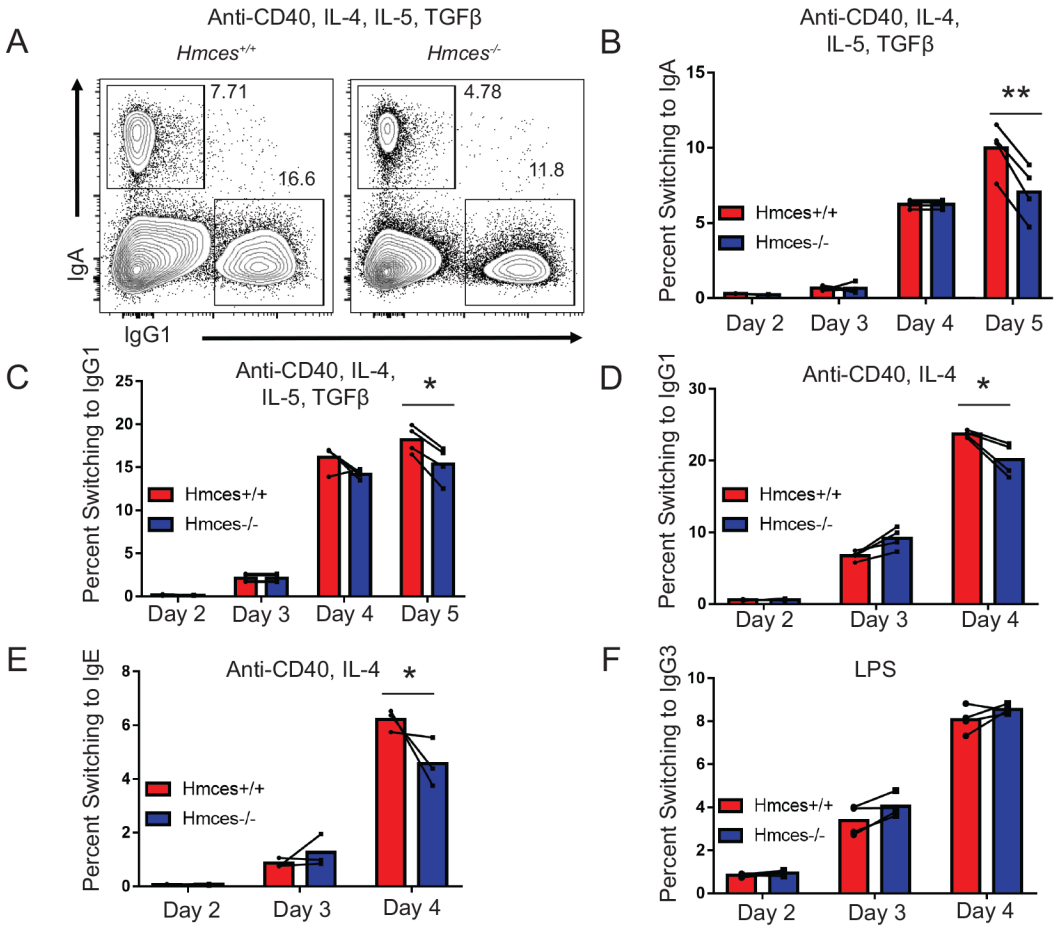

Figure 2: HMCES leads to a B cell intrinsic defect in CSR.

A) Representative flow cytometry plots showing CSR to IgG1 and IgA in B cells isolated from *Hmces*$^{+/+}$ and *Hmces*$^{-/-}$ mice and stimulated with anti-CD40, IL-4, TGF-β and IL-5 for 5 days. **B)** Bar graphs quantifying the kinetics of IgM to IgA switching in primary B cells from *Hmces*$^{+/+}$ and *Hmces*$^{-/-}$ mice. **C)** Bar graphs quantifying the kinetics of IgM to IgG1 switching in primary B cells isolated from *Hmces*$^{+/+}$ and *Hmces*$^{-/-}$ mice stimulated with anti-CD40, IL-4, TGF-β and IL-5. **D)** Bar graphs quantifying the kinetics of IgM to IgG1 switching in primary B cells isolated from *Hmces*$^{+/+}$ and *Hmces*$^{-/-}$ mice and stimulated with anti-CD40 and IL-4. **E)** Bar graphs quantifying the kinetics of IgM to IgE switching in primary B cells isolated from *Hmces*$^{+/+}$ and *Hmces*$^{-/-}$ mice and stimulated with anti-CD40 and IL-4. **F)** Bar graphs quantifying the kinetics of IgM to IgG3 switching in primary B cells isolated from *Hmces*$^{+/+}$ and *Hmces*$^{-/-}$ mice and stimulated with LPS. Data are represented as mean ± SD. Each dot represents cells isolated from an individual mouse and lines are used to highlight samples analyzed in the same experiment. Statistical significance was calculated using two-way ANOVA. *p value ≤0.005, **p value ≤0.001.

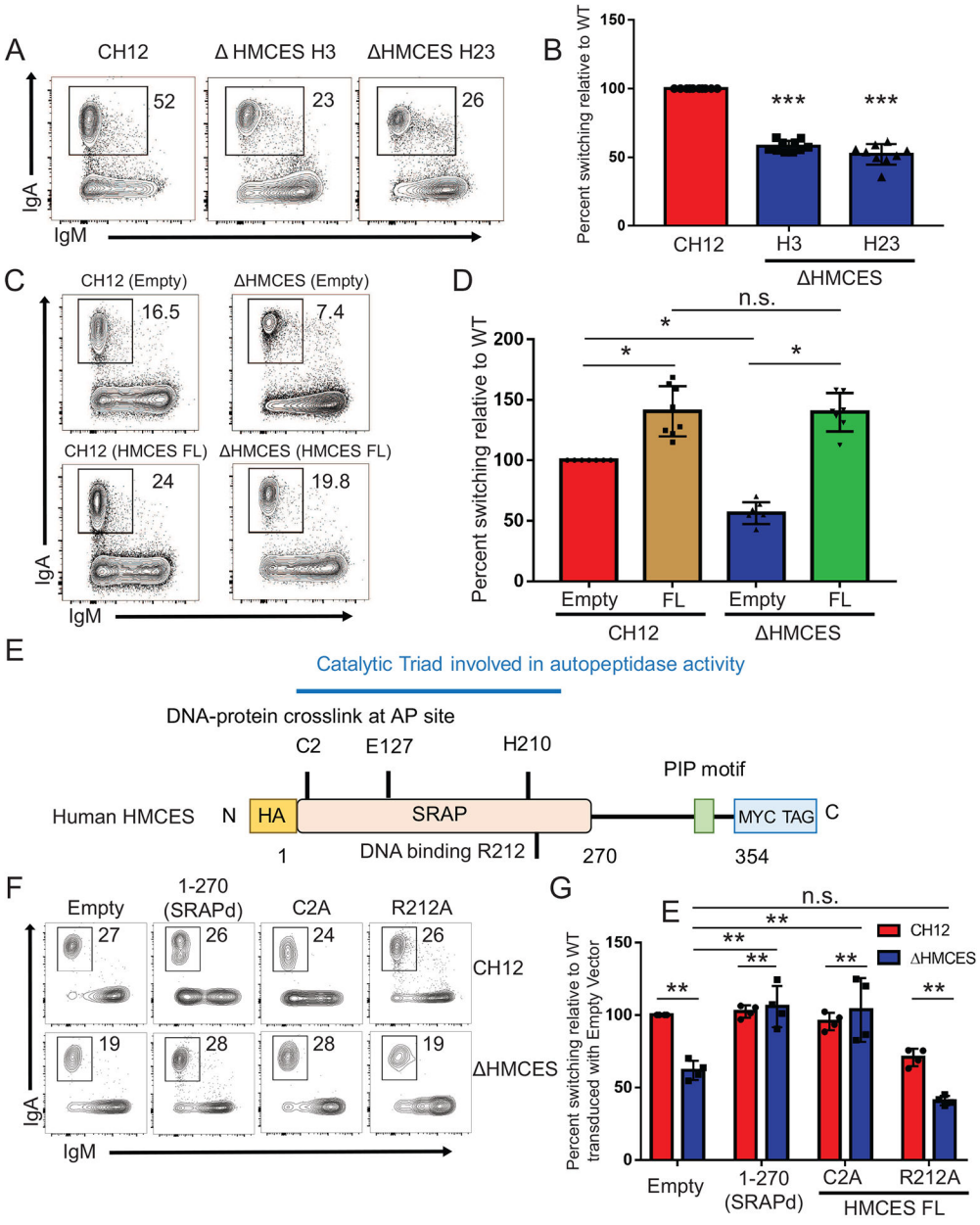

Figure 3: HMCES deficiency leads to a defect in CSR in the CH12 B cell line.

A) Representative flow cytometry plots of WT or ΔHMCES CH12 cells (clones H3 and H23). Cells were stimulated with anti-CD40, Interleukin-4 (IL-4) and Transforming growth factor-β (TGF-β) (CIT) and CSR from IgM to IgA was measured after 72 hours. **B)** Bar graph showing the relative percent CSR in ΔHMCES CH12 clones H3 and H23 compared with WT CH12 cells after 72 hours of CIT stimulation. **C)** Flow cytometry plots showing the frequency of CSR to IgA after 72 hours of CIT stimulation in WT and ΔHMCES CH12 cells transduced with either empty lentiviral vector or vector expressing full length (FL) HMCES protein. The ΔHMCES plot is representative of both H3 and H23 ΔHMCES CH12 cells. **D)** Bar graphs showing the relative percent CSR in ΔHMCES CH12 cells, normalized to WT CH12 cells transduced with empty vector in the same experiment. Data from H3 and

H23 ΔHMCES CH12 cells are merged. **E)** Diagram indicating selected known features of human HMCES protein tested with the mutational analysis. **F)** Flow cytometry plots showing the frequency of CSR to IgA after 72 hours of CIT stimulation in WT and ΔHMCES CH12 cells transduced with either empty lentiviral vector or vectors expressing HMCES 1–270 (SRAPd), HMCES C2A or HMCES R212A variants generated on FL HMCES backbone. The ΔHMCES plot is representative of both H3 and H23 ΔHMCES CH12 cells. **G)** Bar graph showing the relative percent CSR of WT or ΔHMCES (both H3 and H23) CH12 cells lentivirally transduced with empty vector, HMCES 1–270 (SRAPd), HMCES C2A and HMCES R212A variant proteins generated on. CSR is normalized to WT CH12 cells transduced with empty vector in the same experiment. Data are representative of 4 or more independent experiments with each dot representing an independent experiment. Data are represented as mean ± SD. Statistical significance was calculated using student t-test. ***p value ≤0.000001, *p value ≤0.001 (panels B and D) or by two-way ANOVA **p value ≤0.0001 (panel G).

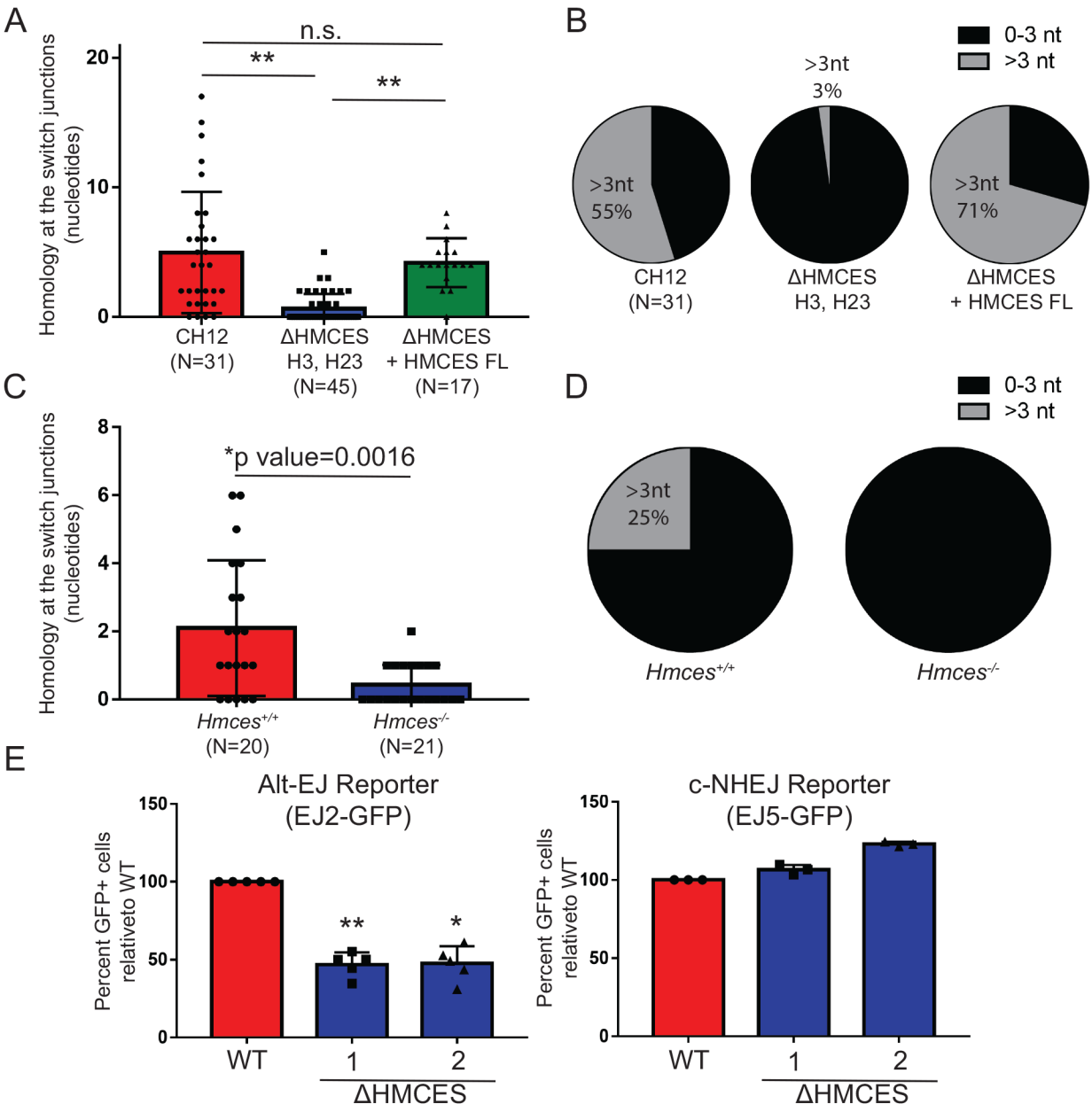

Figure 4: HMCES deficiency results in defects in DNA DSB repair through the microhomology-mediated alternative end-joining pathway.

A) Bar graphs quantifying the distribution of observed microhomologies in Sμ-Sα switch junctions of WT CH12, ΔHMCES CH12 clones H3 and H23, and ΔHMCES CH12 clone H3 reconstituted with FL HMCES protein (detected by PCR amplification and Sanger sequencing). Data are representative of two independent experiments. Statistical significance was computed using Welch's T-test. **B)** Pie charts displaying distribution of Sμ-Sα switch region microhomologies of 0–3 or >3 nucleotides in WT CH12, ΔHMCES CH12 clones H3 and H23, and ΔHMCES CH12 clone H3 reconstituted with FL HMCES. Cells were stimulated with anti-CD40, Interleukin-4 (IL-4) and Transforming growth factor-β (TGF-β) for 72 hours. **C)** Bar graphs quantifying the distribution of observed microhomologies in Sμ-

Sγ1 switch junctions of *Hmces*$^{+/+}$ and *Hmces*$^{-/-}$ primary B cells (detected by PCR amplification and Sanger sequencing) stimulated with anti-CD40 and IL-4 for 4 days. Data are representative of two independent experiments. Statistical significance was computed using Welch's T-test. **D)** Pie charts displaying distribution of Sμ-Sγ1 switch junctional microhomologies of 0–3 or >3 nucleotides in *Hmces*$^{+/+}$ and *Hmces*$^{-/-}$ primary B cells stimulated with anti-CD40 and IL-4 for 4 days. **E)** Bar graphs showing the relative percentage of GFP-positive cells in ΔHMCES U2OS-EJ2-Alt-EJ reporter cells (*left*) or ΔHMCES U2OS-EJ5-cNHEJ reporter cells (*right*) compared with corresponding WT U2OS reporter cells. Data are represented as mean ± SD and are representative of at least three independent experiments. Statistical significance was calculated using student t-test. **p value ≤0.0001, *p value ≤0.0005.

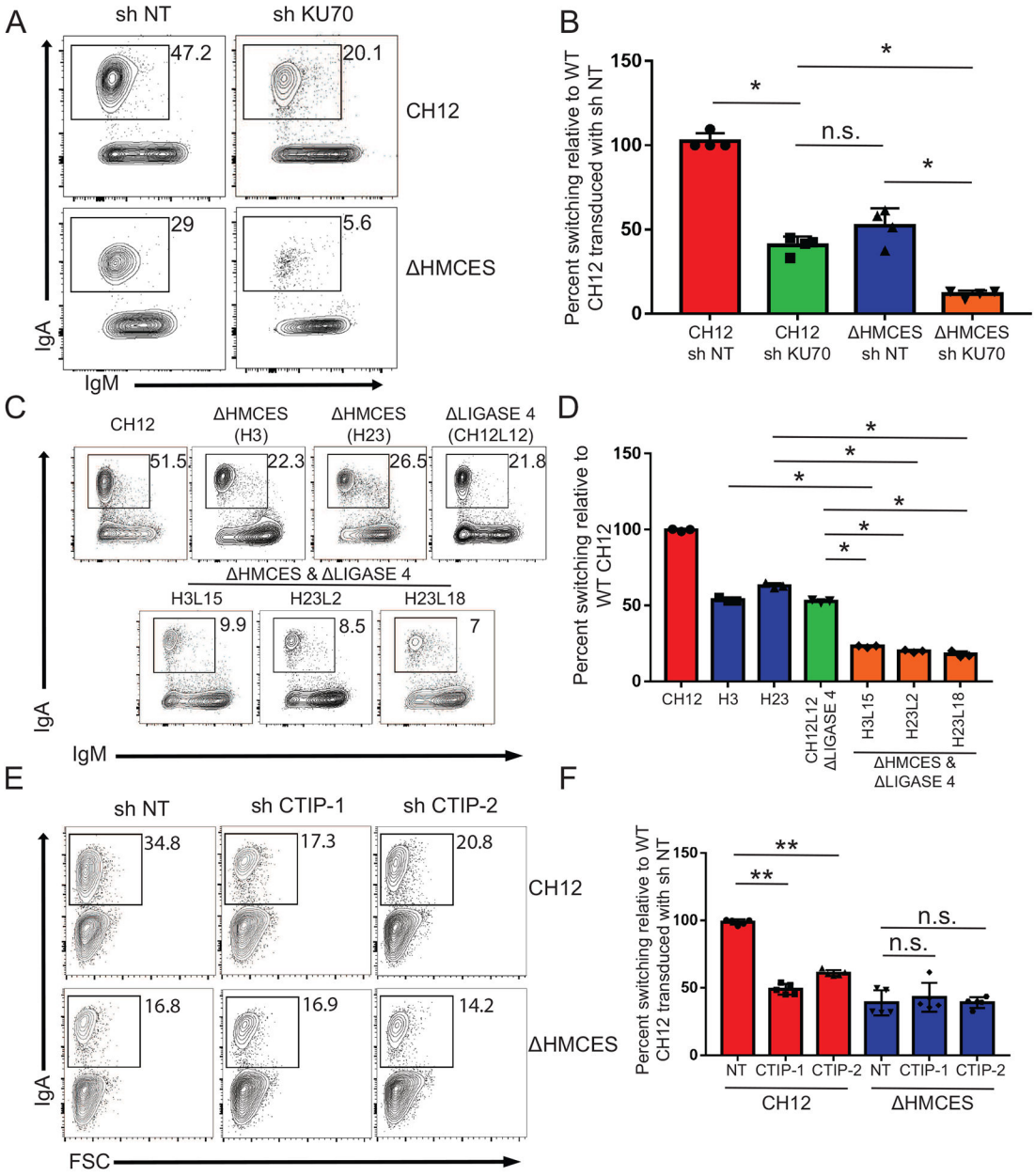

Figure 5: Genetic disruption of c-NHEJ in HMCES-deficient CH12 cells results in a striking decrease in DNA DSB repair.

A) Representative flow cytometry plots showing CSR to IgA in CH12 shNT, CH12 shKU70, ΔHMCES shNT and ΔHMCES shKU70 cells stimulated with anti-CD40, Interleukin-4 (IL-4) and Transforming growth factor-β (TGF-β) (CIT) for 72 hours. **B)** Bar graphs quantifying the relative percent of CSR to IgA in WT or ΔHMCES (H23) CH12 cells lentivirally transduced with a non-targeting shRNA (shNT) or shRNA against KU70 (shKU70). Percent switching is normalized to WT CH12 cells transduced with shNT in each experiment. **C)** Representative flow cytometry plots showing CSR to IgA in WT, ΔHMCES (H3 and H23), ΔLIGASE4 (CH12 L12) and, ΔHMCES and LIGASE4 double-deficient CH12 cells (H3 L15, H23 L2, H23 L18) after 72 hours stimulation with CIT. **D)** Bar graphs

quantifying the relative percent CSR to IgA in WT, ΔHMCES (H3 and H23), ΔLIGASE4 (CH12 L12) and, ΔHMCES and LIGASE4 double-deficient CH12 cells (H3 L15, H23 L2, H23 L18). **E)** Representative flow cytometry plots showing switching to IgA in CH12 shNT, CH12 shCTIP-1, ΔHMCES shNT, ΔHMCES shCTIP-1 and ΔHMCES shCTIP-2 cells stimulated with CIT for 72 hours. **F)** Bar graphs quantifying CSR to IgA in WT or ΔHMCES (H23) CH12 cells lentivirally transduced with a non-targeting shRNA (shNT) or shRNAs against CTIP (shCTIP-1 and shCTIP-2). Percent switching is normalized to WT CH12 cells transduced with shNT in each experiment. Data in panels B and D are represented as mean ± SD and each dot represents an independent experiment. Statistical significance was calculated using student t-test. *p value ≤0.0005, **p value ≤0.00001.

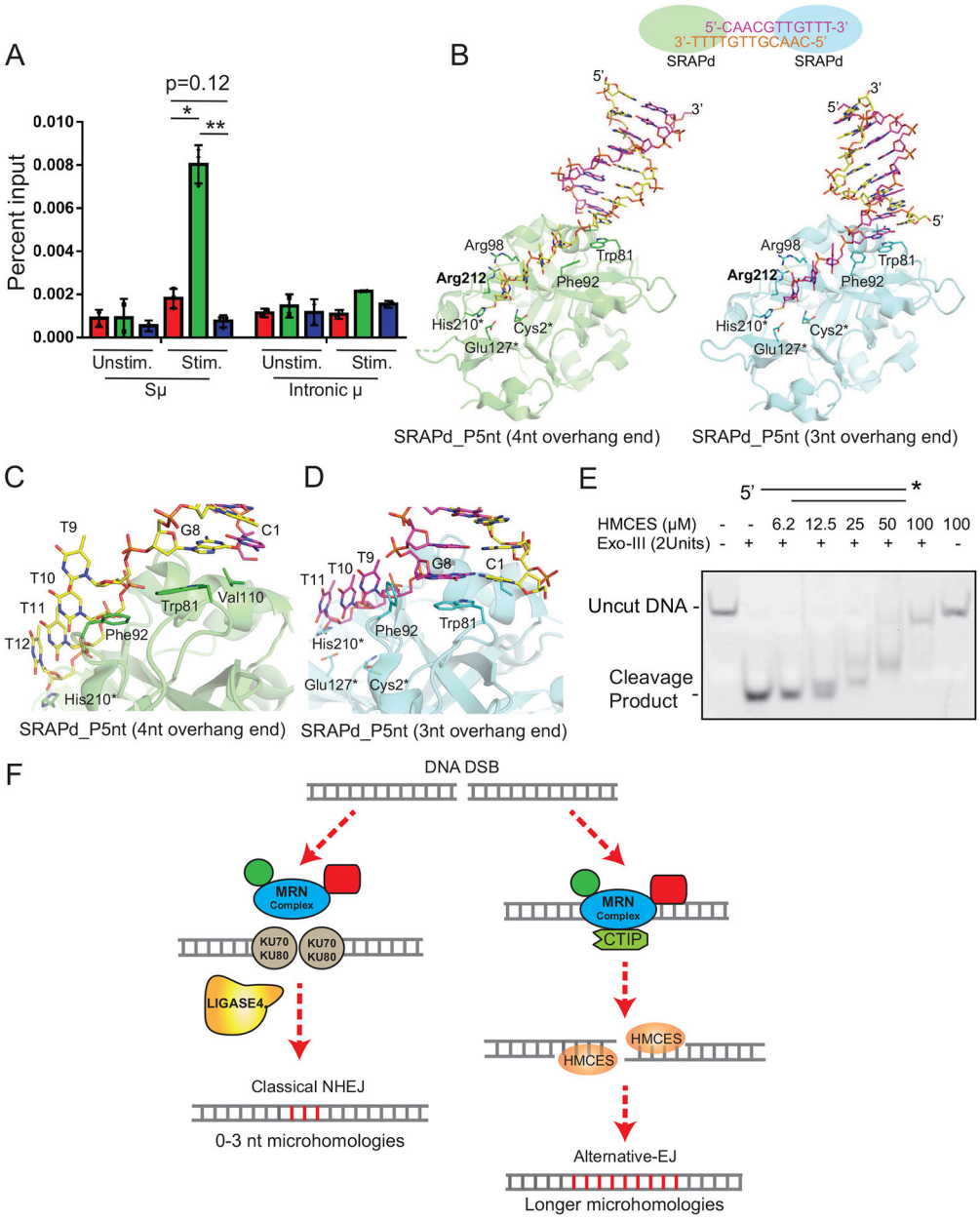

Figure 6: HMCES binds switch regions and protects ssDNA overhangs during CSR.

A) ChIP qRT-PCR showing recruitment of HMCES to switch μ region DNA but not to an adjacent intronic μ enhancer region in WT or KU70 knockdown CH12 cells upon stimulation with anti-CD40, IL-4 and TGFβ. ΔHMCES CH12 (clone H23) cells were used as negative control. Data are representative of 3 or more independent experiments. Data are represented as mean ± SD. Statistical significance was calculated using student t-test. **p value ≤0.002, *p value ≤0.01. **B)** Co-crystal structure of the human HMCES SRAP domain (SRAPd) in complex with palindromic DNA flanked by 3-nucleotide *(left)* or 4-nucleotide *(right)* overhangs at each 3' end. (SRAPd_P5nt; PDB ID: 6OOV). DNA is shown in stick model (Yellow and magenta). SRAPd is shown in cartoon representation and colored green (left) and cyan (right). The catalytic triad residues are marked with an asterisk. **C)** A

zoomed-in view of the SRAPd interaction site with 3-nucleotide overhang in SRAPd_P5nt. **D)** A zoomed-in view of the SRAPd interaction site with a 4-nucleotide overhang in SRAPd_P5nt. **E)** Polyacrylamide gel image of the exonuclease protection assay of a 5' overhang DNA incubated with serially diluted human HMCES SRAPd. * represents 6-carboxyfluorescein (6FAM). The data are representative of two independent experiments. **F)** A model describing the postulated role of HMCES in DNA DSB repair during CSR.

Key Resources Table

REAGENT or RESOURCE	SOURCE	IDENTIFIER
Antibodies		
anti-HMCES Antibody	Santa Cruz Biotechnology	#sc-514238, RRID:AB_281385
anti-KU70 antibody	Santa Cruz Biotechnology	#sc-17789, RRID:AB_628454
anti-LIGASE4 antibody	Santa Cruz Biotechnology	#sc-271299, RRID:AB_10610371
anti-CTIP antibody	Santa Cruz Biotechnology	#sc-271339, RRID:AB_10608728
anti-Actin HRP conjugated	Cell Signaling technologies	#5125, RRID:AB_1903890
anti-mouse IgA PE conjugated	Southern Biotechnology	#1040–09, RRID: AB_2794375
anti-mouse IgM APC conjugated	Biolegend	#406509, RRID:
		AB_315059
anti-HA PE conjugated	Biolegend	#901518, RRID:AB_2629623
anti-IgG1 PE conjugated	Biolegend	#406608, RRID: AB_10551618
Chemicals, Peptides, and Recombinant Proteins		
human HMCES SRAPd recombinant protein	this manuscript	
Experimental Models: Cell Lines		
HMCES Knockout CH12F3 cells	this manuscript	
LIGASE 4 Knockout CH12F3 cells	this manuscript	
Experimental Models: Organisms/Strains		
Hmces-defcient mice	Dr. Douglas E. Feldman	PMID:29020633
Oligonucleotides name and Sequences 5’ to 3’		Genomic position
mouse Hmces gRNA 1 F: CACCGGGCAGCGCTGAAGTATGTGC	Integrated DNA technology	Chr6:87914498
mouse Hmces gRNA 1 R: AAACGCACATACTTCAGCGCTGCCC	Integrated DNA technology	
mouse Hmces gRNA 2 F: CACCGCTGCGGGCTCTTGTTGTAGG	Integrated DNA technology	chr6:87914631
mouse Hmces gRNA 2 R: AAACCCTACAACAAGAGCCCGCAGC	Integrated DNA technology	
mouse Lig4 gRNA 1 F: CACCGCTCAATTACCGAACCCCCAG	Integrated DNA technology	Chr8:9973429
mouse Lig4 gRNA 1 R: AAACCTGGGGGTTCGGTAATTGAGC	Integrated DNA technology	
mouse Lig4 gRNA 2 F: CACCGTGGAGATTCACCAAACTGGT	Integrated DNA technology	chr8: 9972861

REAGENT or RESOURCE	SOURCE	IDENTIFIER
mouse Lig4 gRNA 2 R: AAACACCAGTTTGGTGAATCTCCAC	Integrated DNA technology	
human Hmces gRNA 1 F: CACCGGTATCATTGCTCCCATGCGC	Integrated DNA technology	chr3:129288873
human Hmces gRNA 1 R: AAACGCGCATGGGAGCAATGATAC	Integrated DNA technology	
human Hmces gRNA 2 F: CACCGTACGGTATCACTACGACAGT	Integrated DNA technology	chr3: 129288954
human Hmces gRNA 2 R: AAACACTGTCGTAGTGATACCGTAC	Integrated DNA technology	
DNA used for SRAPd P5nt crystal structure: CAACGTTGTTTTT	Integrated DNA technology	
Exonuclease assay Oligonucleotide A: TCGGATTCTTCTGGTCCGGATGGTAGTTAAGT*G*T*T*G*A*G *6-phosphorothioate linkages	Integrated DNA technology	
Exonuclease assay Oligonucleotide B: -/6FAM/-C*T*C*A*A*C*ACTTAACTACCATCCGGACCAGAAGA *6-phosphorothioate linkages	Integrated DNA technology	
Recombinant DNA		
pLV-EF1a-IRES GFP-Human HMCES FL	this manuscript	
pLV-EF1a-IRES GFP-Human HMCES 1–270 (SRAPd)	this manuscript	
pLV-EF1a-IRES GFP-Human HMCES C2A	this manuscript	
pLV-EF1a-IRES GFP-Human HMCES R212A	this manuscript	
Co-crystal Structure		
SRAPd_P5nt	this manuscript, deposited in PDB	PDB ID:6OOV
YedK_ssDNA abasic site	PDB	PDB ID: 6NUA Pubmed ID: 31235915
YedK ssDNA	PDB	PDB ID: 6KBS Pubmed ID: 31504793